

DETECTION AND SOURCES OF GRAVITATIONAL WAVES

Rainer Weiss, MIT

New England Particle Physics
Student Retreat IV

Craigville Beach, Mass

August 19, 2005

697

SITZUNGSBERICHTE

1916.

XXXIII.

DER

KÖNIGLICH PREUSSISCHEN

AKADEMIE DER WISSENSCHAFTEN.

688

Sitzung der physikalisch-mathematischen Klasse vom 22. Juni 1916

AS.A. 311

SCIENCE LIBRARY MIT

Näherungsweise Integration der Feldgleichungen
der Gravitation.

Von A. EINSTEIN.

$$\gamma'_{\mu\nu} = \alpha_{\mu\nu} f(x_1 + i x_4) = \alpha_{\mu\nu} f(x - t). \quad (15)$$

Dabei sind die $\alpha_{\mu\nu}$ Konstante; f ist eine Funktion des Arguments $x - t$. Ist der betrachtete Raum frei von Materie, d. h. verschwinden die $T_{\mu\nu}$, so sind die Gleichungen (6) durch diesen Ansatz erfüllt. Die Gleichungen (4) liefern zwischen den $\alpha_{\mu\nu}$ die Beziehungen

$$\left. \begin{aligned} \alpha_{11} + i\alpha_{14} &= 0 \\ \alpha_{12} + i\alpha_{24} &= 0 \\ \alpha_{13} + i\alpha_{34} &= 0 \\ \alpha_{14} + i\alpha_{44} &= 0 \end{aligned} \right\}. \quad (16)$$

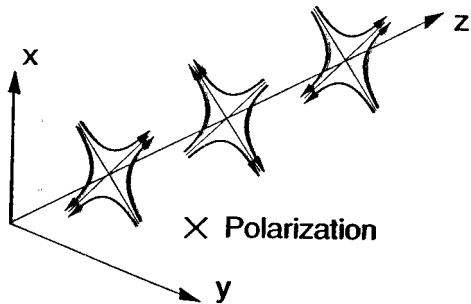
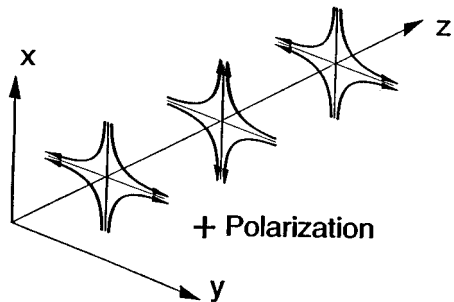
Von den 10 Konstanten $\alpha_{\mu\nu}$ sind daher nur 6 frei wählbar. Wir können die allgemeinste Welle der betrachteten Art daher aus Wellen von folgenden 6 Typen superponieren

$$\left. \begin{array}{lll} \text{a) } \alpha_{11} + i\alpha_{14} = 0 & \text{b) } \alpha_{12} + i\alpha_{24} = 0 & \text{d) } \alpha_{22} \neq 0 \\ \alpha_{14} + i\alpha_{44} = 0 & \text{c) } \alpha_{13} + i\alpha_{34} = 0 & \text{e) } \alpha_{23} \neq 0 \\ & & \text{f) } \alpha_{33} \neq 0 \end{array} \right\}. \quad (17)$$

$$\begin{aligned} \text{d) } \frac{1}{i} t_{22} &= \frac{f'^2}{4\kappa} \alpha_{22}^2 = \frac{1}{4\kappa} \left(\frac{\partial \gamma'_{22}}{\partial t} \right)^2 \\ \text{e) } \frac{1}{i} t_{23} &= \frac{f'^2}{4\kappa} \alpha_{23}^2 = \frac{1}{4\kappa} \left(\frac{\partial \gamma'_{23}}{\partial t} \right)^2 \\ \text{f) } \frac{1}{i} t_{33} &= \frac{f'^2}{4\kappa} \alpha_{33}^2 = \frac{1}{4\kappa} \left(\frac{\partial \gamma'_{33}}{\partial t} \right)^2 \end{aligned}$$

Es ergibt sich also, daß nur die Wellen des letzten Typs Energie transportieren, und zwar ist der Energietransport einer beliebigen ebenen Welle gegeben durch

$$I_x = \frac{1}{i} t_{41} = \frac{1}{4\kappa} \left[\left(\frac{\partial \gamma'_{22}}{\partial t} \right)^2 + 2 \left(\frac{\partial \gamma'_{23}}{\partial t} \right)^2 + \left(\frac{\partial \gamma'_{33}}{\partial t} \right)^2 \right]. \quad (18)$$



Die in (23), (23 a) und (23 b) auftretenden Integrale, welche nichts anderes sind als zeitlich variable Trägheitsmomente, nennen wir im folgenden zur Abkürzung J_{22} , J_{33} , J_{23} . Dann ergibt sich für die Intensität \mathfrak{I}_x der Energiestrahlung aus (18)

$$\mathfrak{I}_x = \frac{\kappa}{64\pi^2 R^2} \left[\left(\frac{\partial^3 J_{22}}{\partial t^3} \right)^2 + 2 \left(\frac{\partial^3 J_{23}}{\partial t^3} \right)^2 + \left(\frac{\partial^3 J_{33}}{\partial t^3} \right)^2 \right]. \quad (20)$$

SPHERICALLY SYMMETRIC MOTION RADIATES GRAVITATIONAL WAVES

1918

VI VII VIII

SITZUNGSBERICHTE

DER

KÖNIGLICH PREUSSISCHEN

AKADEMIE DER WISSENSCHAFTEN

Sitzung der physikalisch-mathematischen Klasse am 7. Februar. (S. 139)

Sitzung der philosophisch-historischen Klasse am 7. Februar. (S. 141)

J. KIRCHNER: Archon Euthios. (S. 142)

Gesamtsitzung am 14. Februar. (S. 153)

EINSTEIN: Über Gravitationswellen. (Mitteilung vom 31. Januar.) (S. 154)

E. FREUNDLICH: Über die singulären Stellen der Lösungen des n -Körper-Problems. 1. Mitteilung.
(Mitteilung vom 31. Januar.) (S. 168)

BERLIN 1918

VERLAG DER KÖNIGLICHEN AKADEMIE DER WISSENSCHAFTEN

IN KOMMISSION BEI GEORG REIMER

Über Gravitationswellen.

Von A. EINSTEIN.

(Vorgelegt am 31. Januar 1918 [s. oben S. 79].)

Die wichtige Frage, wie die Ausbreitung der Gravitationsfelder erfolgt, ist schon vor anderthalb Jahren in einer Akademiarbeit von mir behandelt worden¹. Da aber meine damalige Darstellung des Gegenstandes nicht genügend durchsichtig und außerdem durch einen bedauerlichen Rechenfehler verunstaltet ist, muß ich hier nochmals auf die Angelegenheit zurückkommen.

Wie damals beschränke ich mich auch hier auf den Fall, daß das betrachtete zeiträumliche Kontinuum sich von einem »galileischen« nur sehr wenig unterscheidet. Um für alle Indizes

$$g_{\mu\nu} = -\delta_{\mu\nu} + \gamma_{\mu\nu} \quad (1)$$

Sind die Bedingungen (15) erfüllt, so stellt (14) eine mögliche Gravitationswelle dar. Um deren physikalische Natur genauer zu durchschauen, berechnen wir deren Dichte des Energiestromes $\frac{t_{41}}{i}$. Durch Einsetzen der in (15) gegebenen $\gamma_{\mu\nu}^i$ in Gleichung (9) erhält man

$$\frac{t_{41}}{i} = \frac{1}{4\kappa} f'^2 \left[\left(\frac{\alpha_{22} - \alpha_{33}}{2} \right)^2 + \alpha_{23}^2 \right]. \quad (16)$$

$$\mathfrak{I}_{uv} = \int x_u x_v \rho dV_0 \quad (23)$$

gesetzt; \mathfrak{I}_{uv} sind die Komponenten des (zeitlich variablen) Trägheitsmomentes des materiellen Systems.

Auf analogem Wege erhält man

$$\int (T_{22} - T_{33}) dV_0 = \frac{1}{2} (\ddot{\mathfrak{I}}_{22} - \ddot{\mathfrak{I}}_{33}). \quad (24)$$

Aus (7a) ergibt sich auf Grund von (22) und (24)

$$\gamma'_{23} = - \frac{\kappa}{4 \pi R} \ddot{\mathfrak{I}}_{23}. \quad (25)$$

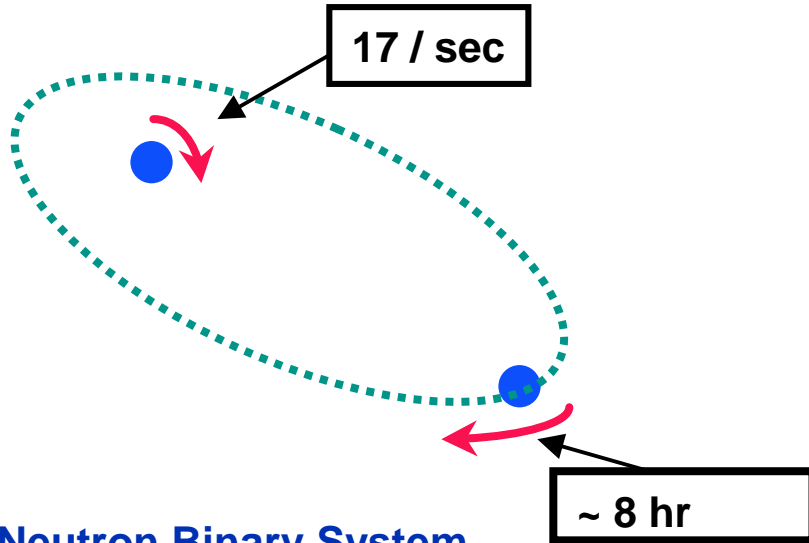
$$\frac{\gamma'_{22} - \gamma'_{33}}{2} = - \frac{\kappa}{4 \pi R} \left(\frac{\ddot{\mathfrak{I}}_{22} - \ddot{\mathfrak{I}}_{33}}{2} \right). \quad (26)$$

Die \mathfrak{I}_{uv} sind nach (7a), (22), (24) für die Zeit $t - R$ zu nehmen, also Funktionen von $t - R$, oder bei großem R in der Nähe der x -Achse auch Funktionen von $t - x$. (25), (26) stellen also Gravitationswellen dar, deren Energiefluß längs der x -Achse gemäß (16) die Dichte

$$\frac{t_{41}}{i} = \frac{\kappa}{64 \pi^2 R^2} \left[\left(\frac{\ddot{\mathfrak{I}}_{22} - \ddot{\mathfrak{I}}_{33}}{2} \right)^2 + \ddot{\mathfrak{I}}_{23}^2 \right] \quad (27)$$

Neutron Binary System – Hulse & Taylor

PSR 1913 + 16 -- Timing of pulsars



Neutron Binary System

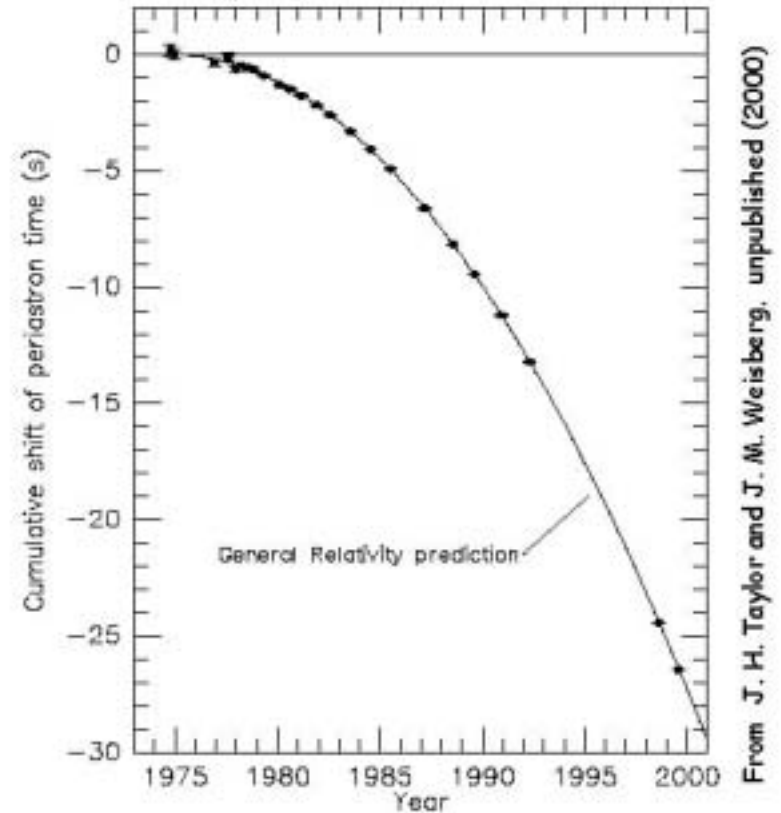
- separated by 10^6 miles
- $m_1 = 1.4m_{\odot}$; $m_2 = 1.36m_{\odot}$; $\varepsilon = 0.617$

Prediction from general relativity

- spiral in by 3 mm/orbit
- rate of change orbital period

Emission of gravitational waves

Comparison between observations of the binary pulsar PSR1913+16, and the prediction of general relativity based on loss of orbital energy via gravitational waves



Direct detection of gravitational waves from astrophysical sources

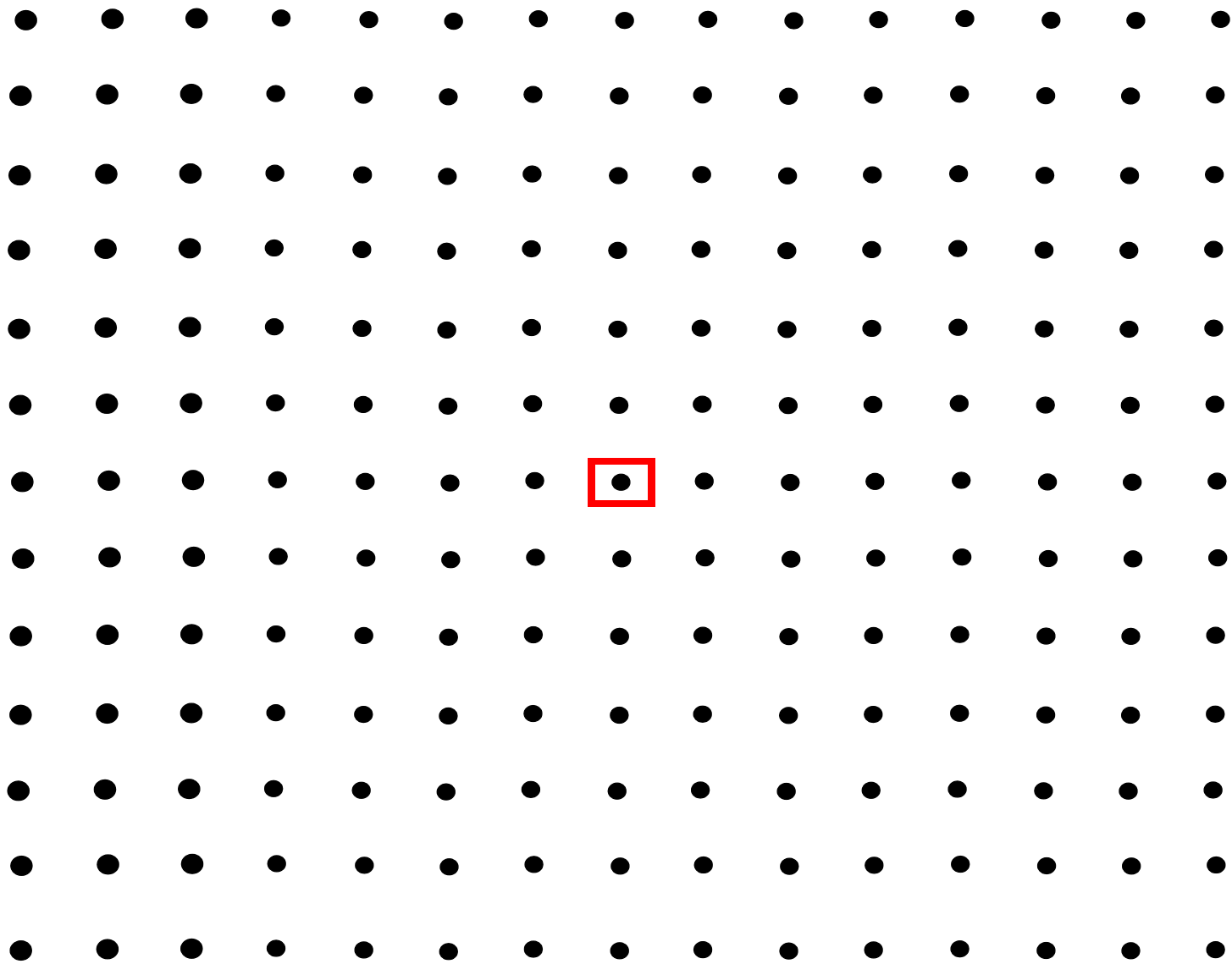
□ Physics

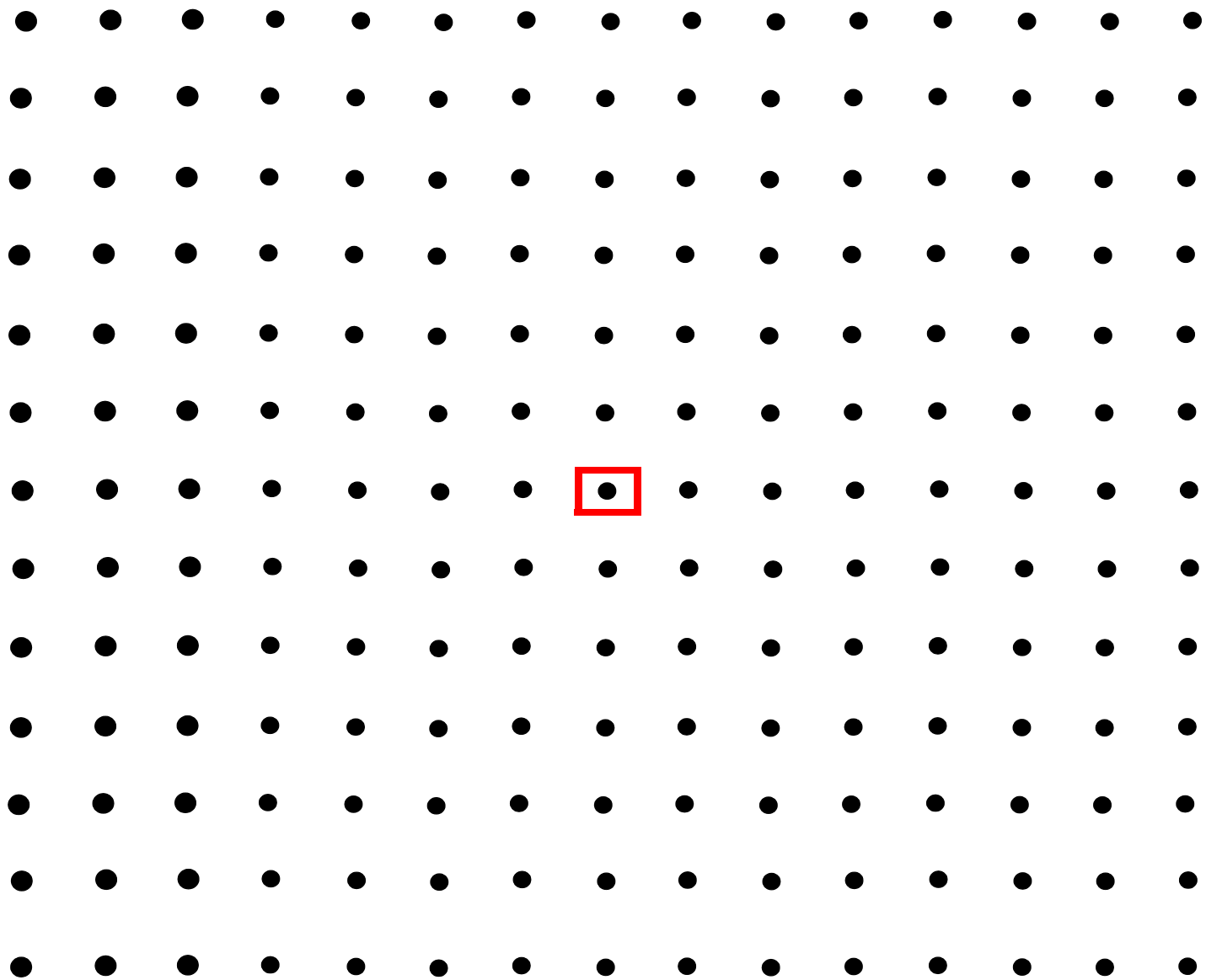
- » Observations of gravitation in the strong field, high velocity limit
- » Determination of wave kinematics – polarization and propagation
- » Tests for alternative relativistic gravitational theories

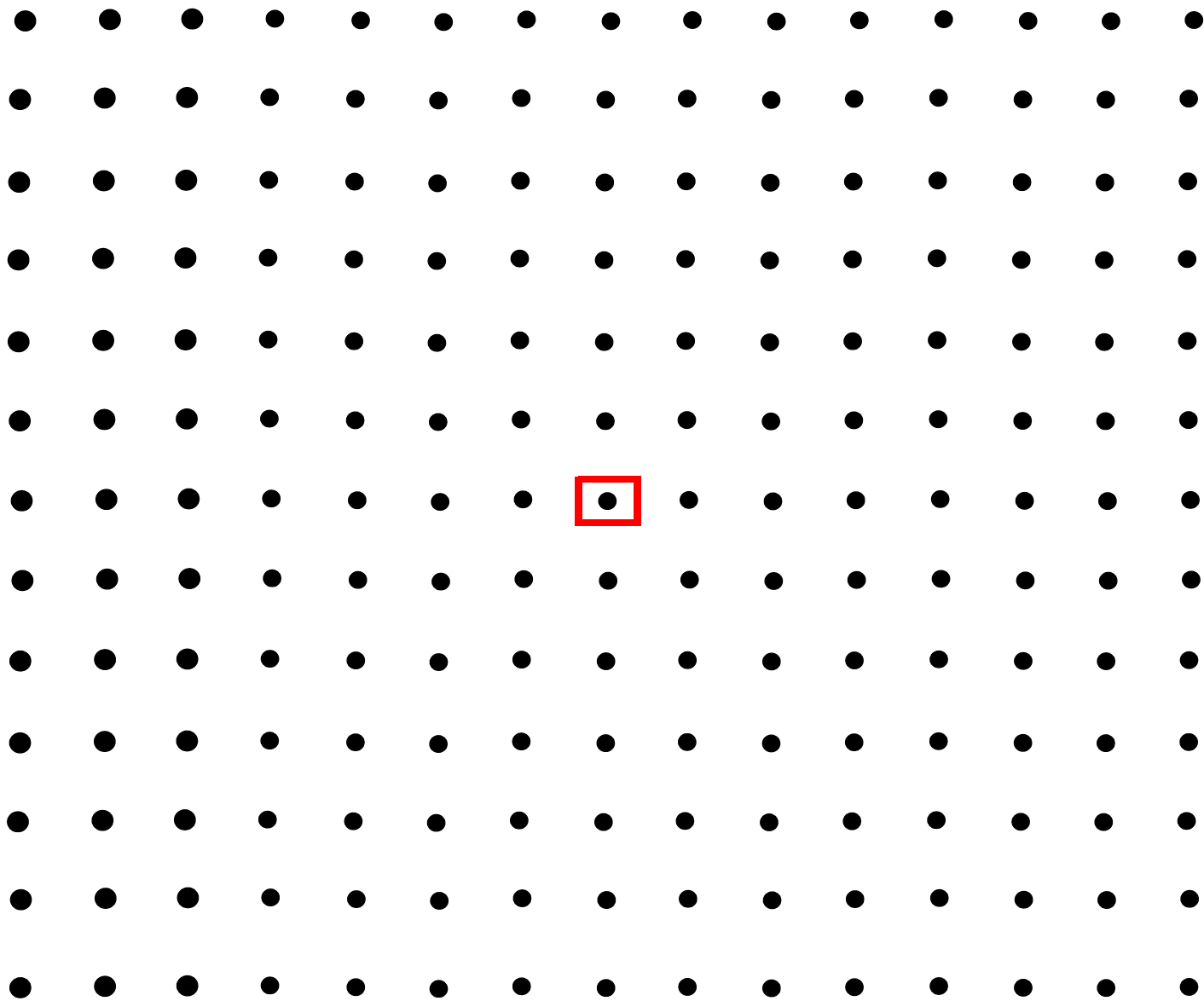
□ Astrophysics

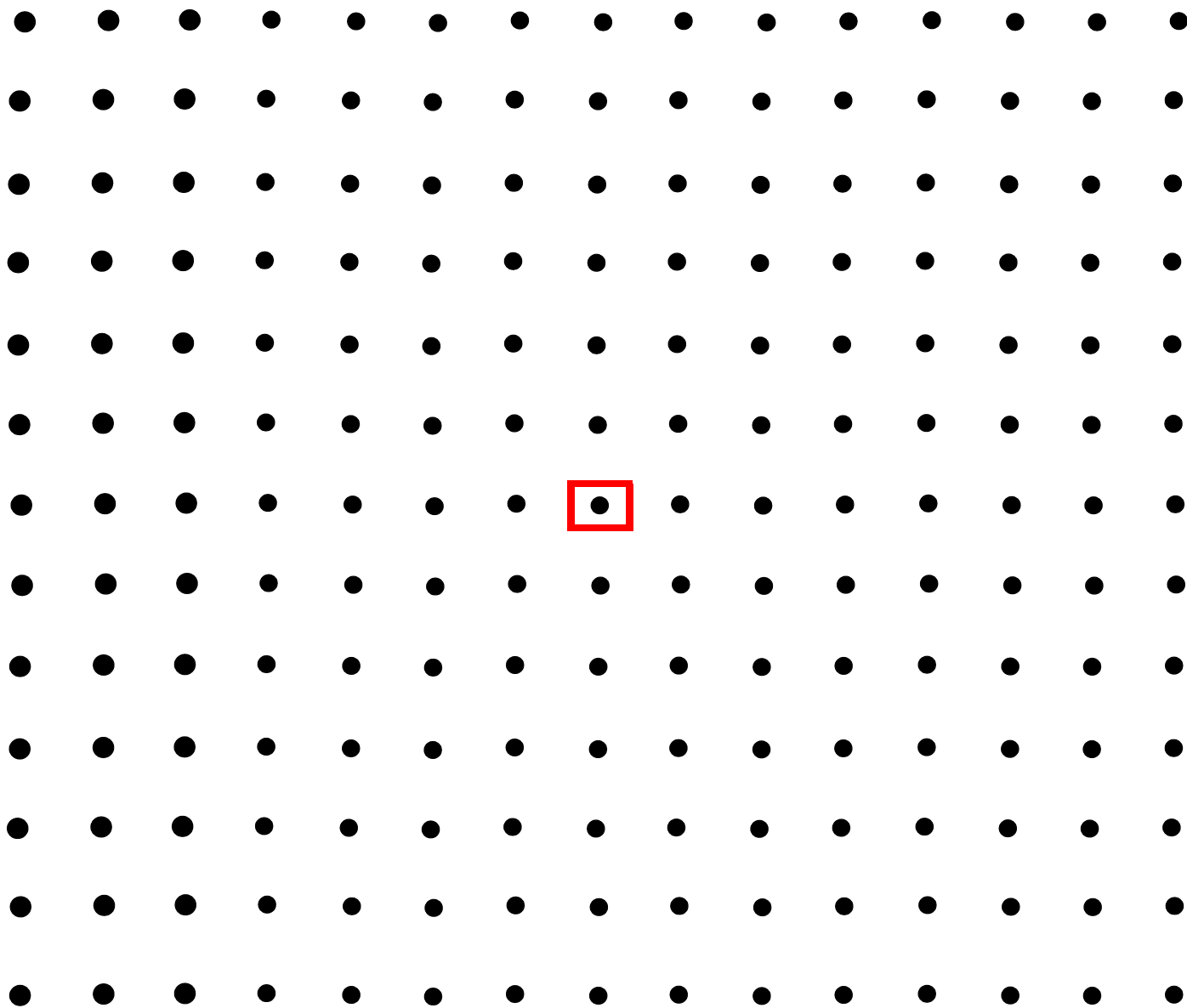
- » Measurement of coherent inner dynamics – stellar collapse, pulsar formation....
- » Compact binary coalescence – neutron star/neutron star, black hole/black hole
- » Neutron star equation of state
- » Primeval cosmic spectrum of gravitational waves

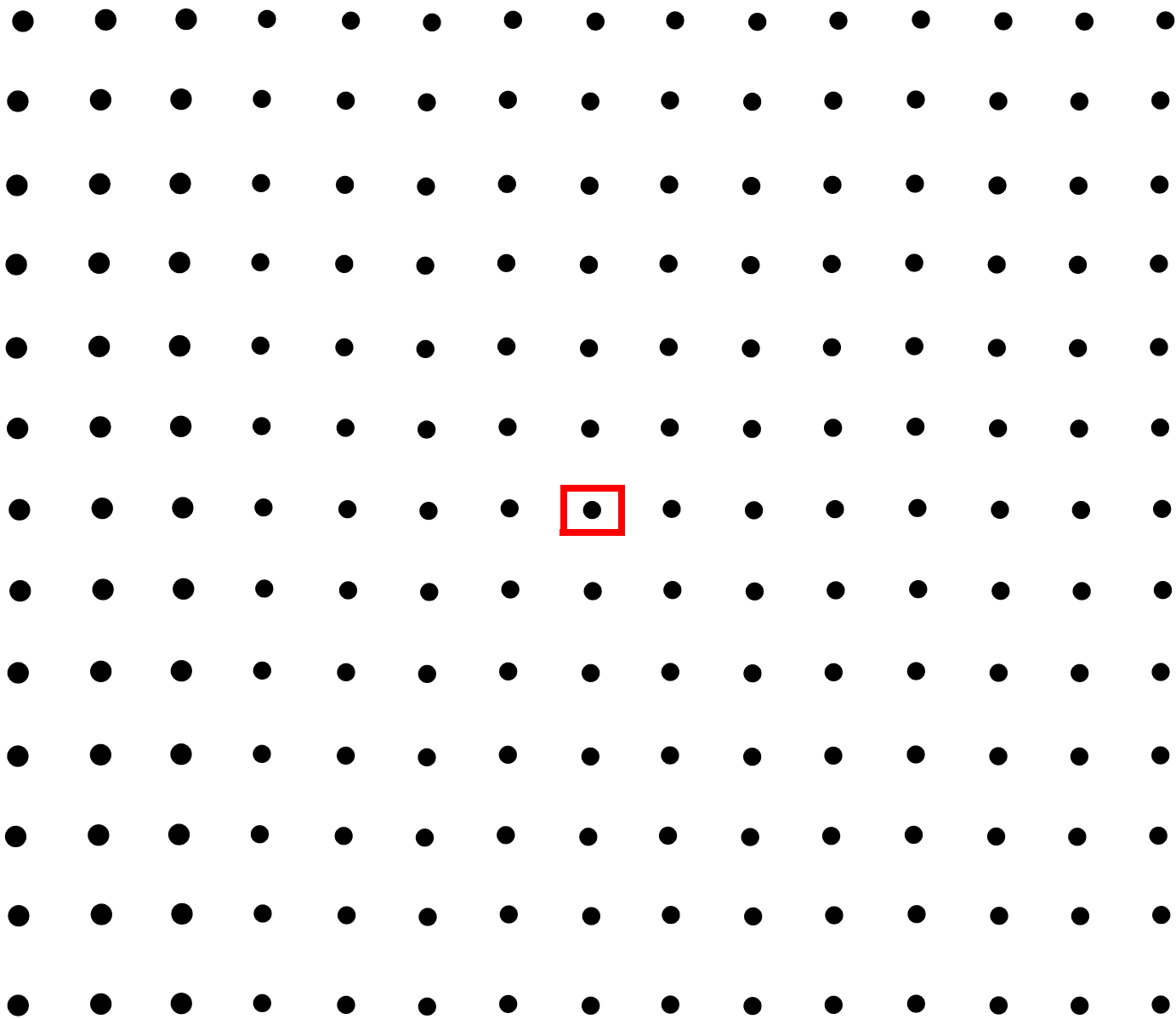
□ Gravitational wave survey of the universe

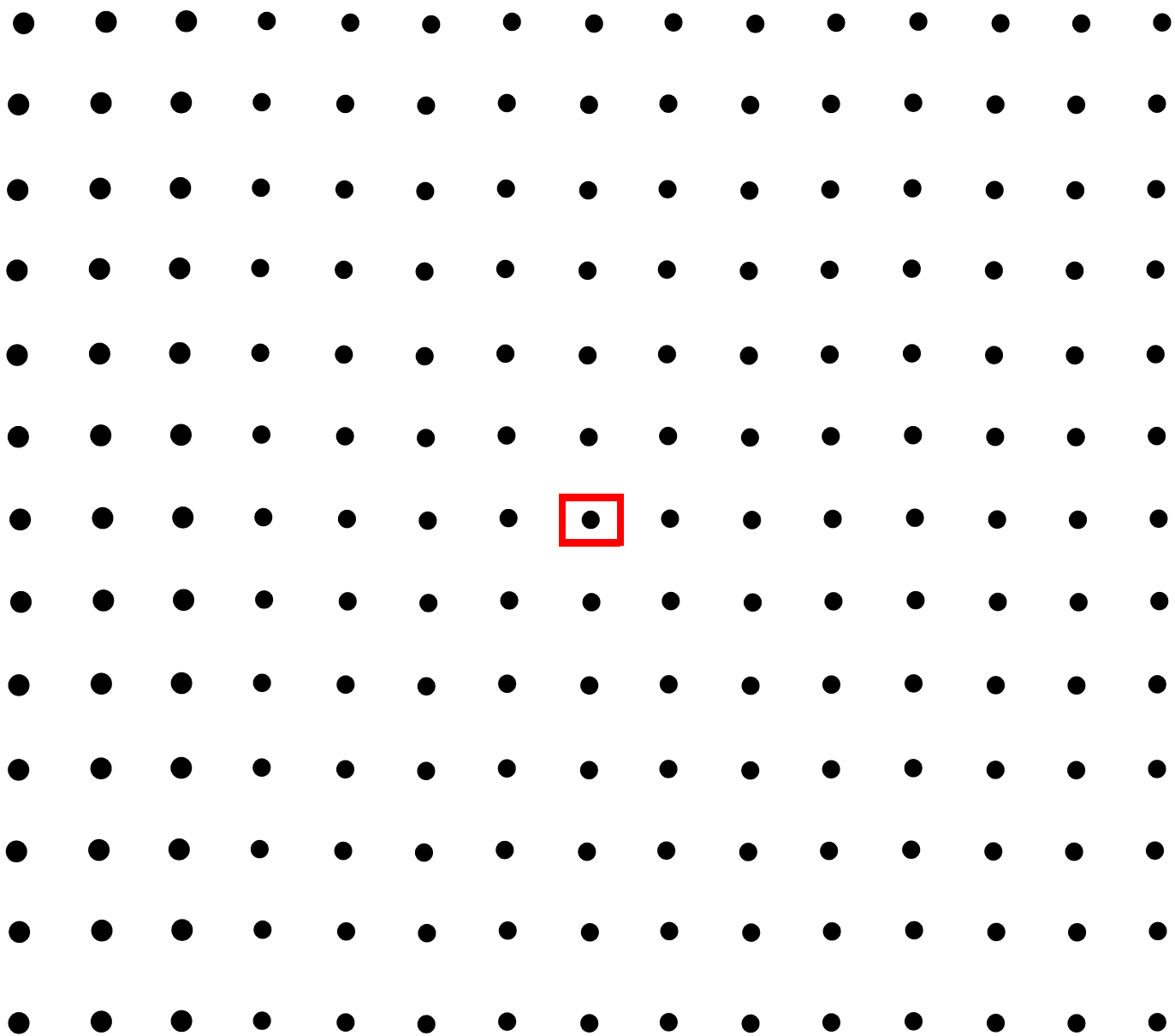


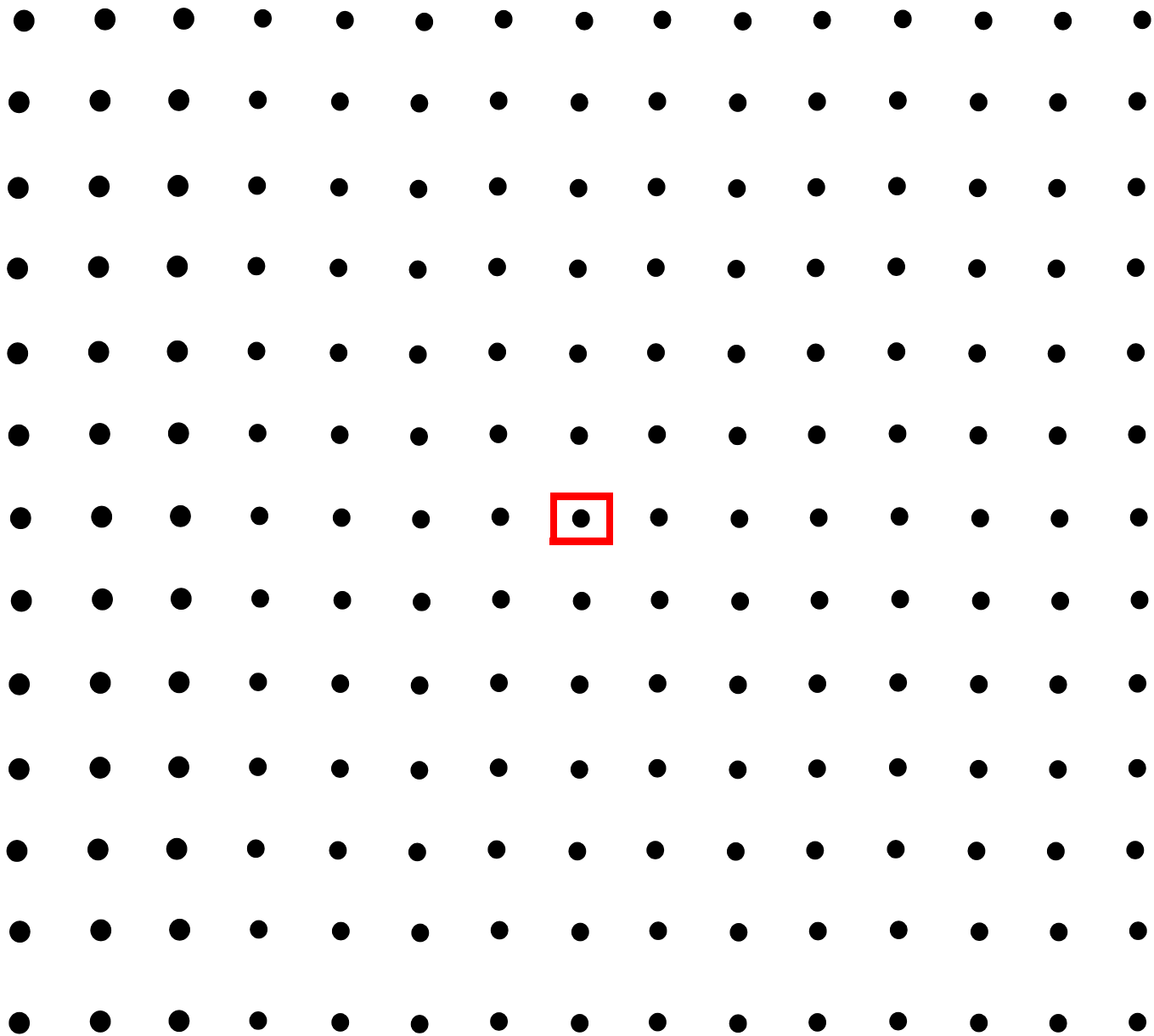


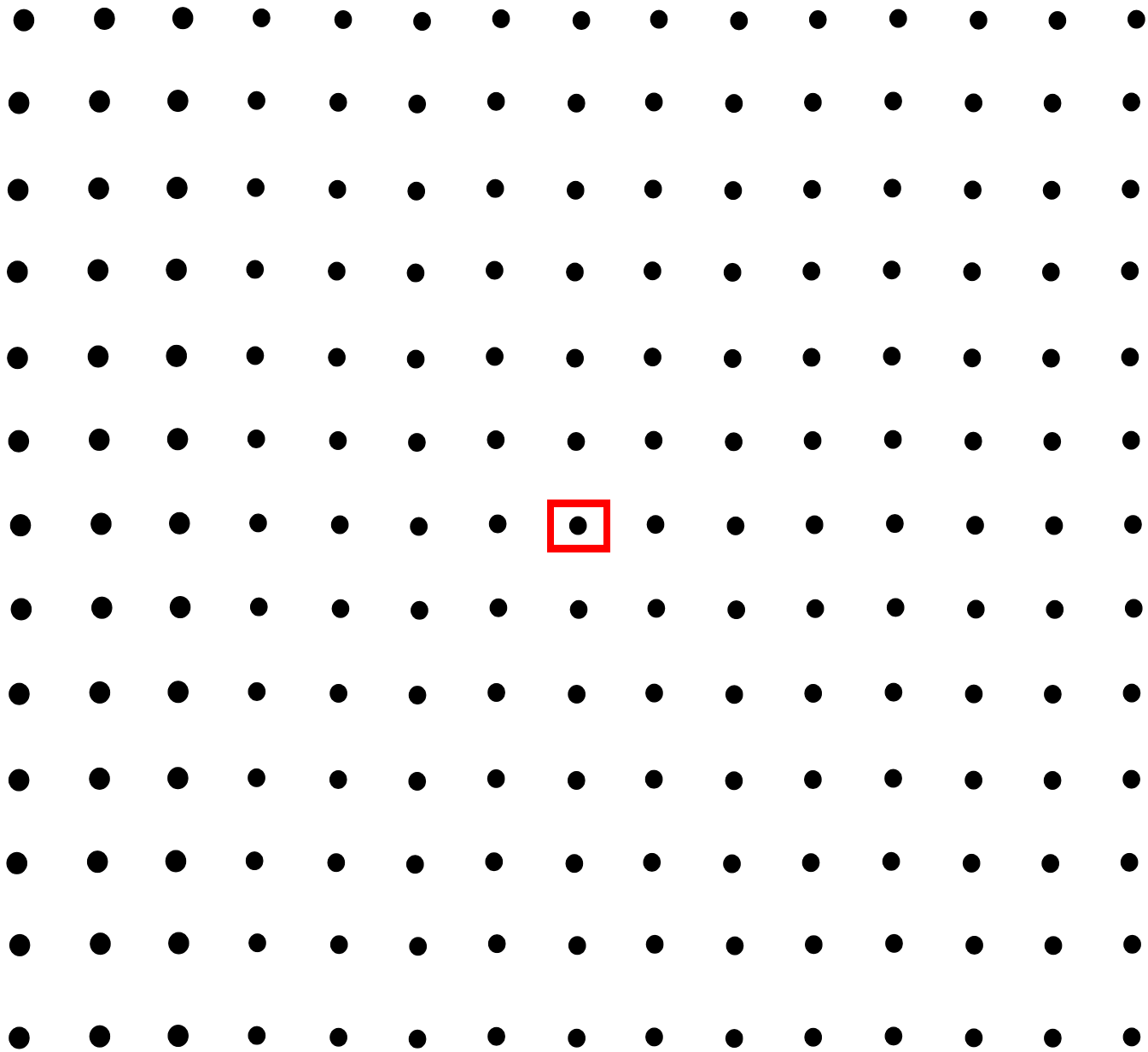


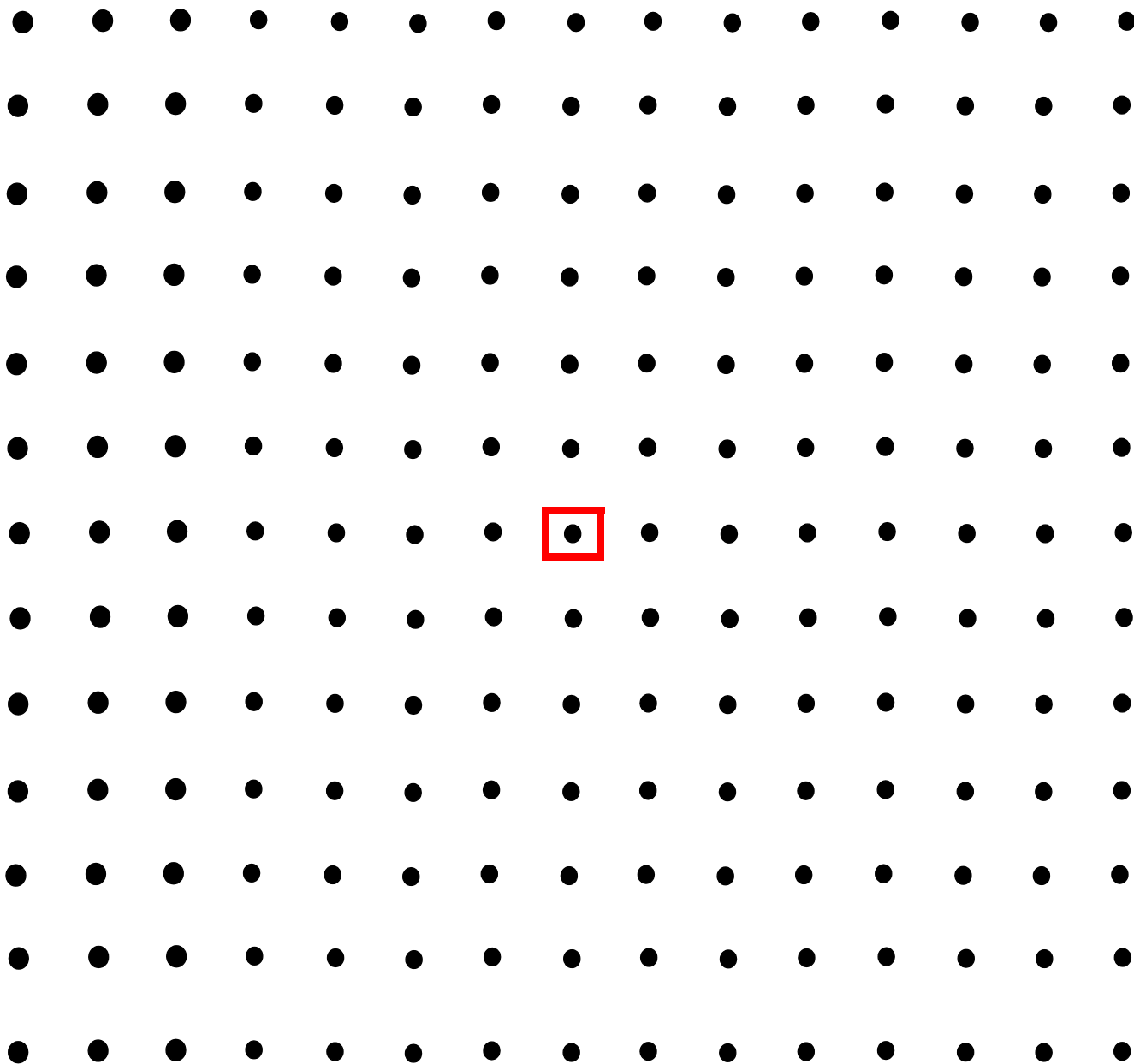


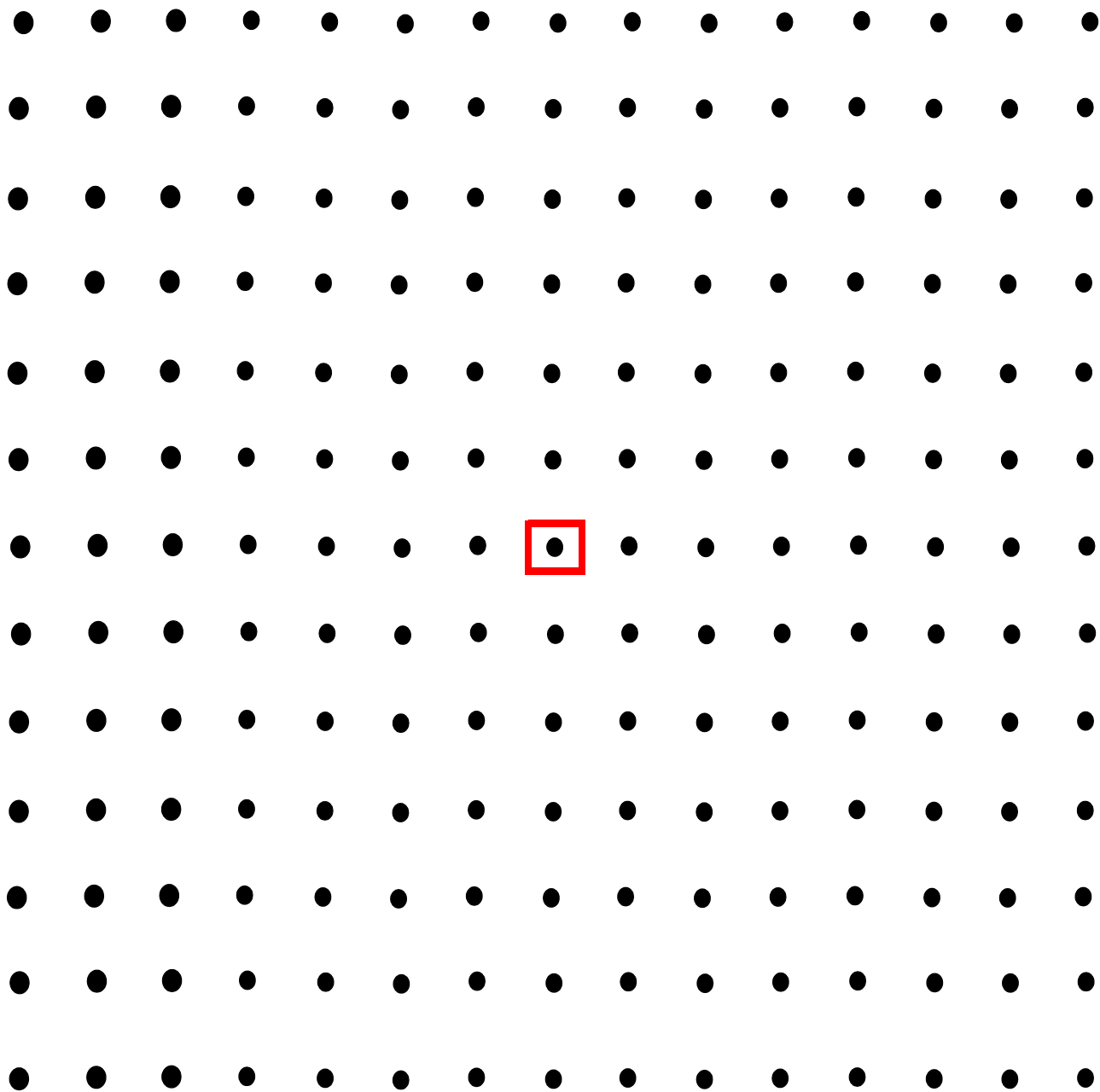


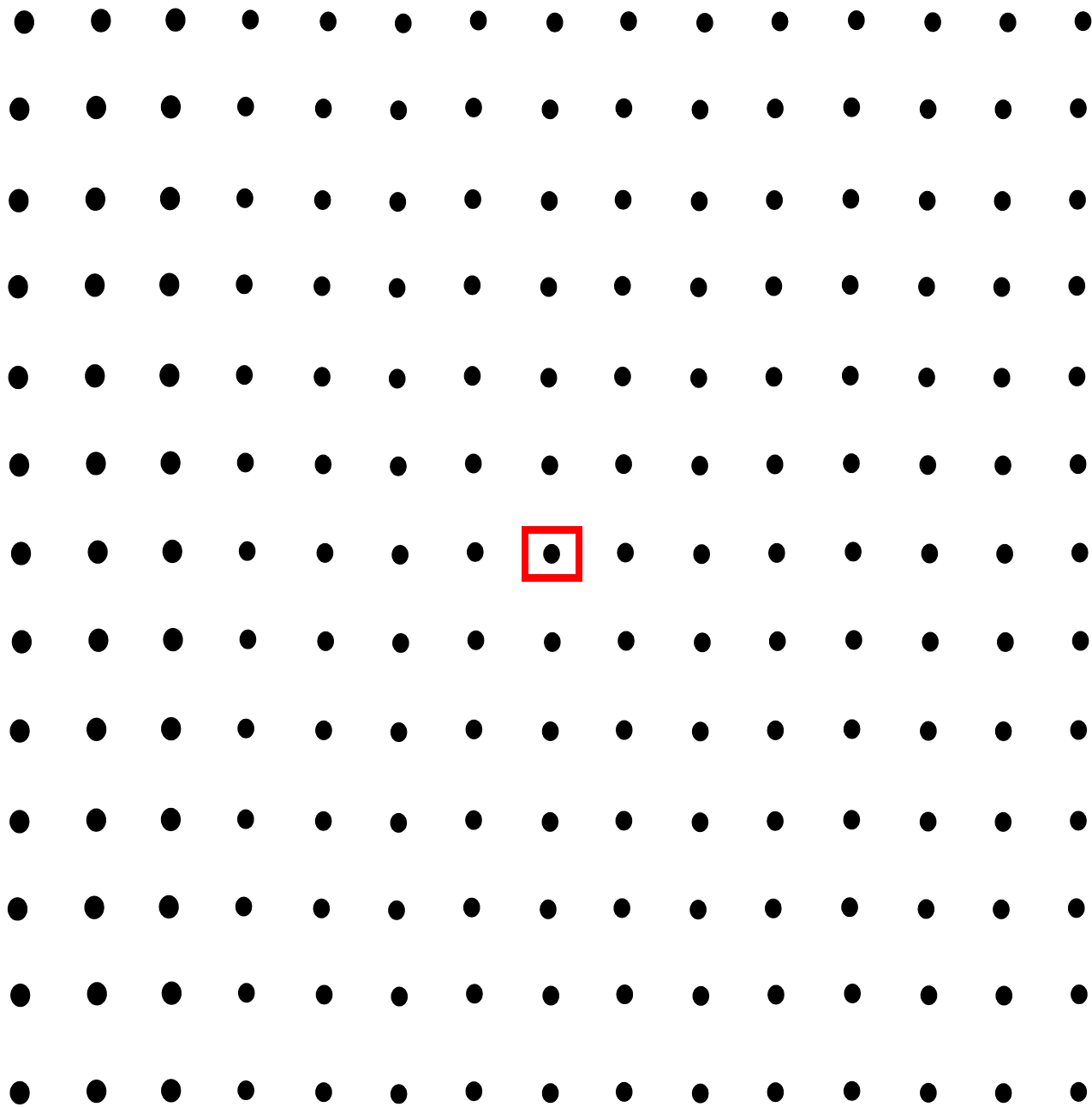


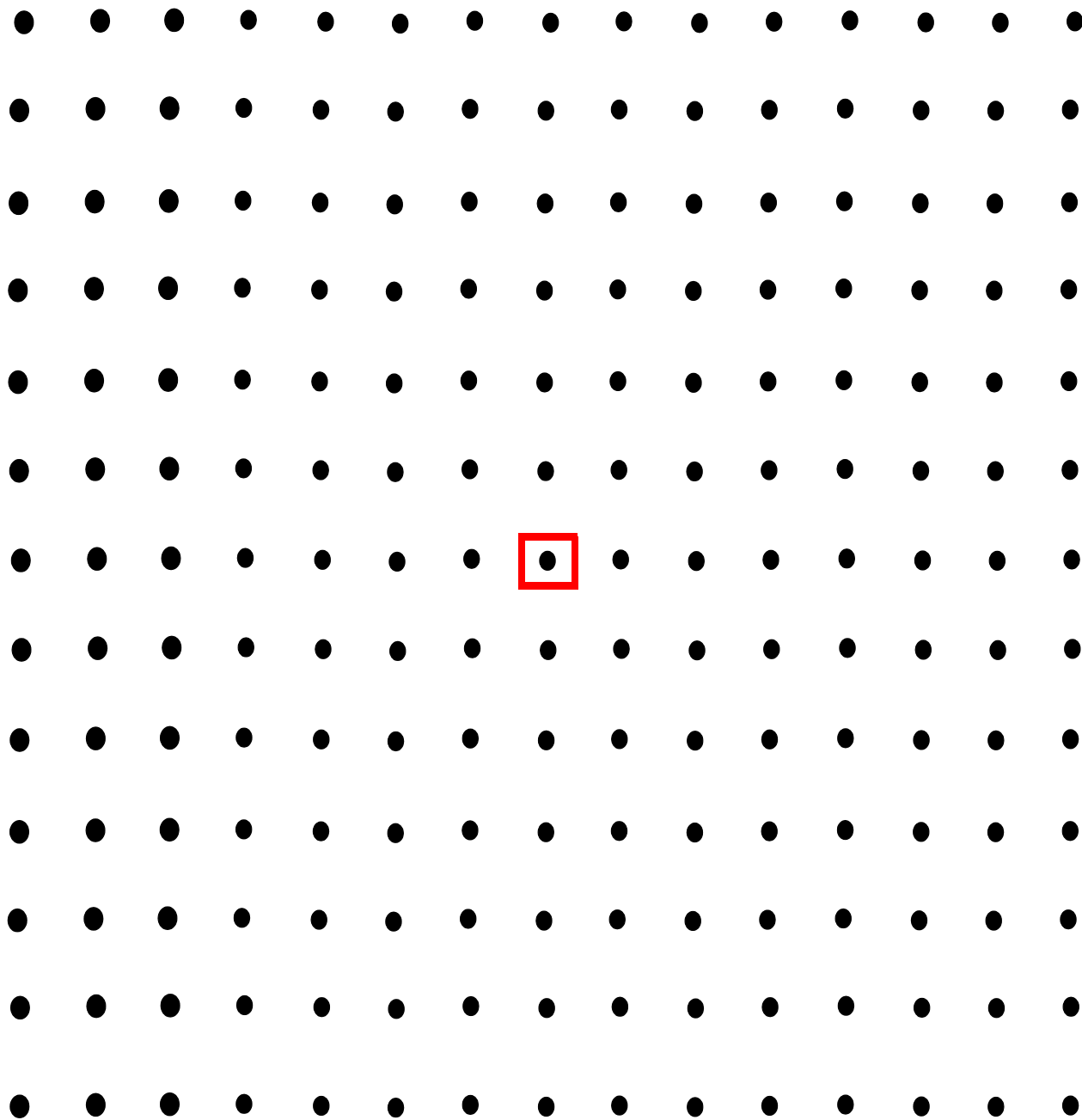


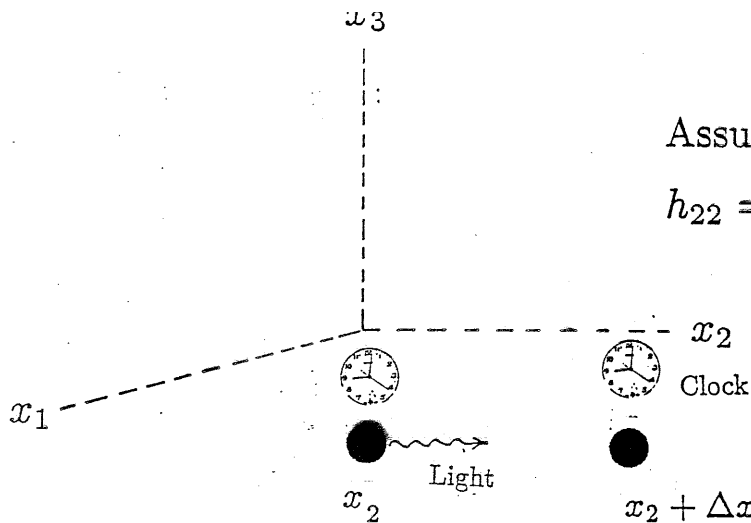












Assume + Polarization

$$h_{22} = h \sin(kx_1 - \omega t)$$

Gravity Wave \downarrow MINKOWSKI

$$\Delta s^2 = 0 = c^2 \Delta t^2 - \left(1 + h \sin(kx_1 - \omega t)\right) \Delta x_2^2$$

LIGHT RAY

Let $\Delta t \ll \frac{1}{\omega} \quad h \ll 1$

$$c \Delta t \cong \left(1 + \frac{h}{2} \sin(kx_1 - \omega t)\right) \Delta x_2$$

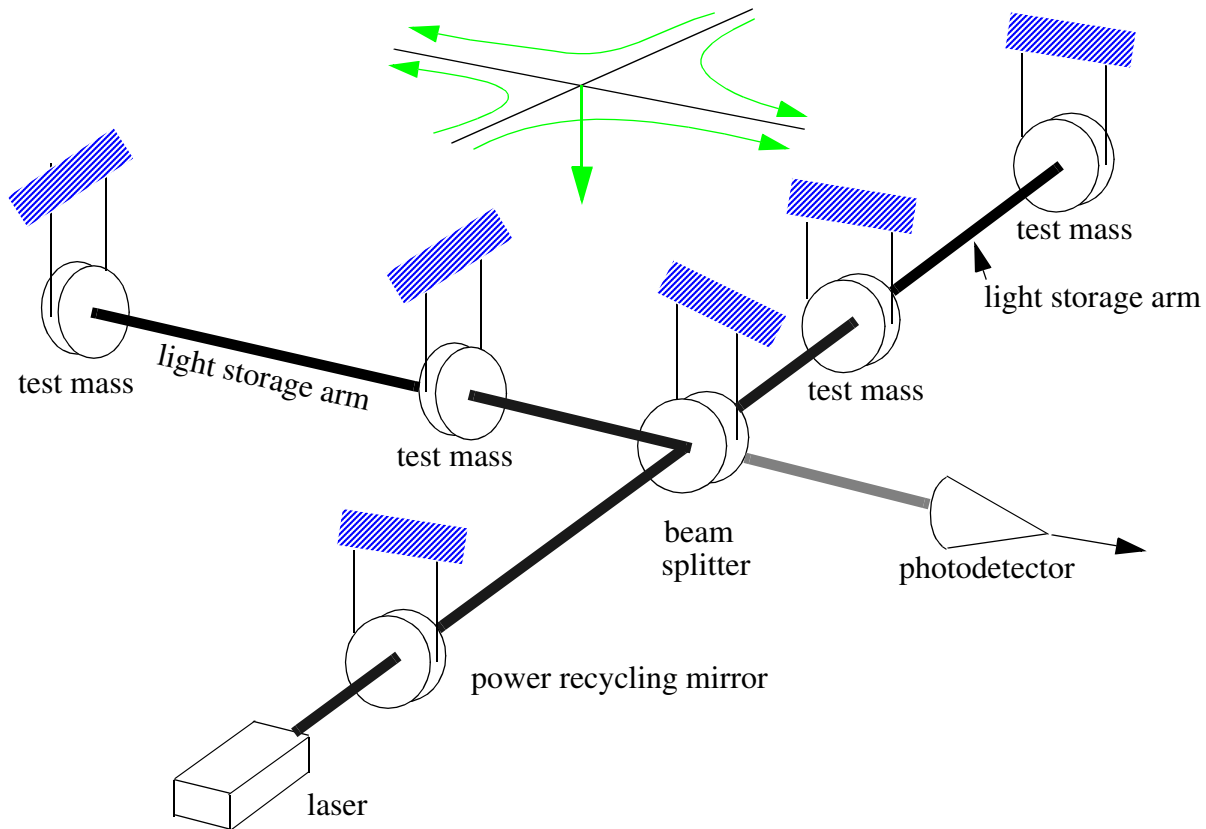
\nwarrow INFERRED
DISTANCE
BETWEEN POINTS

$$\frac{\delta(c \Delta t)}{\Delta x_2} = \frac{h}{2} \sin(kx_1 - \omega t)$$

Time Dependent Strain

$$\frac{\Delta l}{l} = \frac{h}{2}$$

The Measurable Quantity



Measurement challenge

- Needed technology development to measure:

$$h = \Delta L/L < 10^{-21}$$

$$\Delta L < 4 \times 10^{-18} \text{ meters}$$

FRINGE SENSING

$$h = \frac{x}{L} \sim \frac{\lambda}{Lb \sqrt{N\tau}}$$

wavelength $1 \times 10^{-6} \text{ m}$

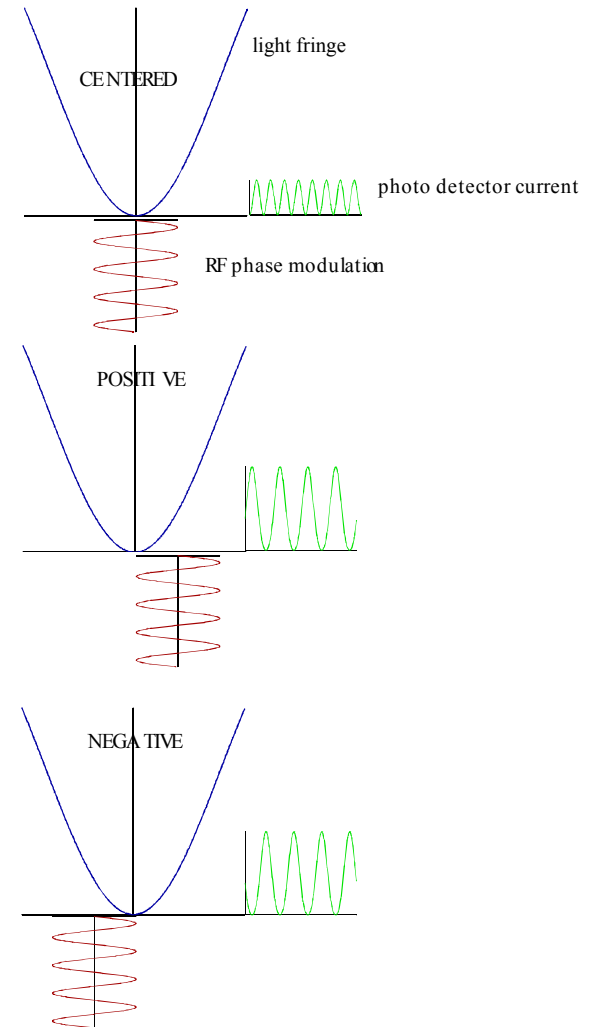
arm length = 4000 m

equivalent # of passes = 100

integration time

number of quanta/second at the beam splitter
 300 watts at beam splitter = 10^{21} identical photons/sec

$$h = 6 \times 10^{-22} \quad \text{integration time } 10^{-2} \text{ sec}$$



PENDULUM THERMAL NOISE

Pendulum Brownian motion

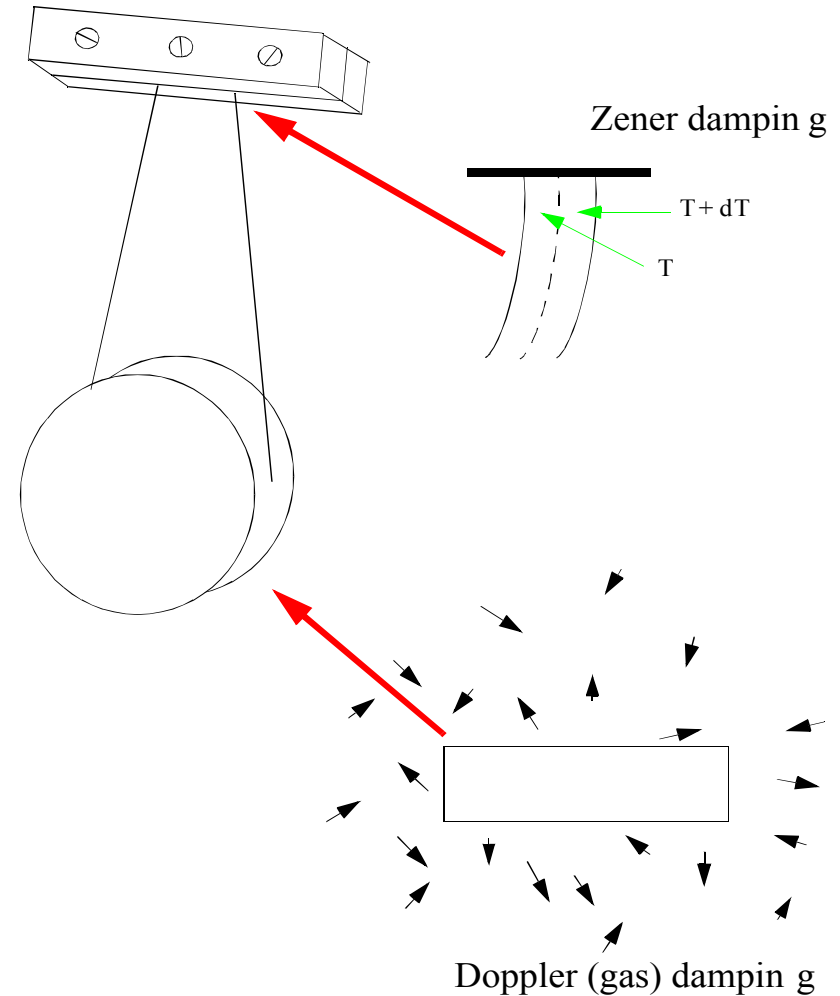
Dissipation leads to fluctuations

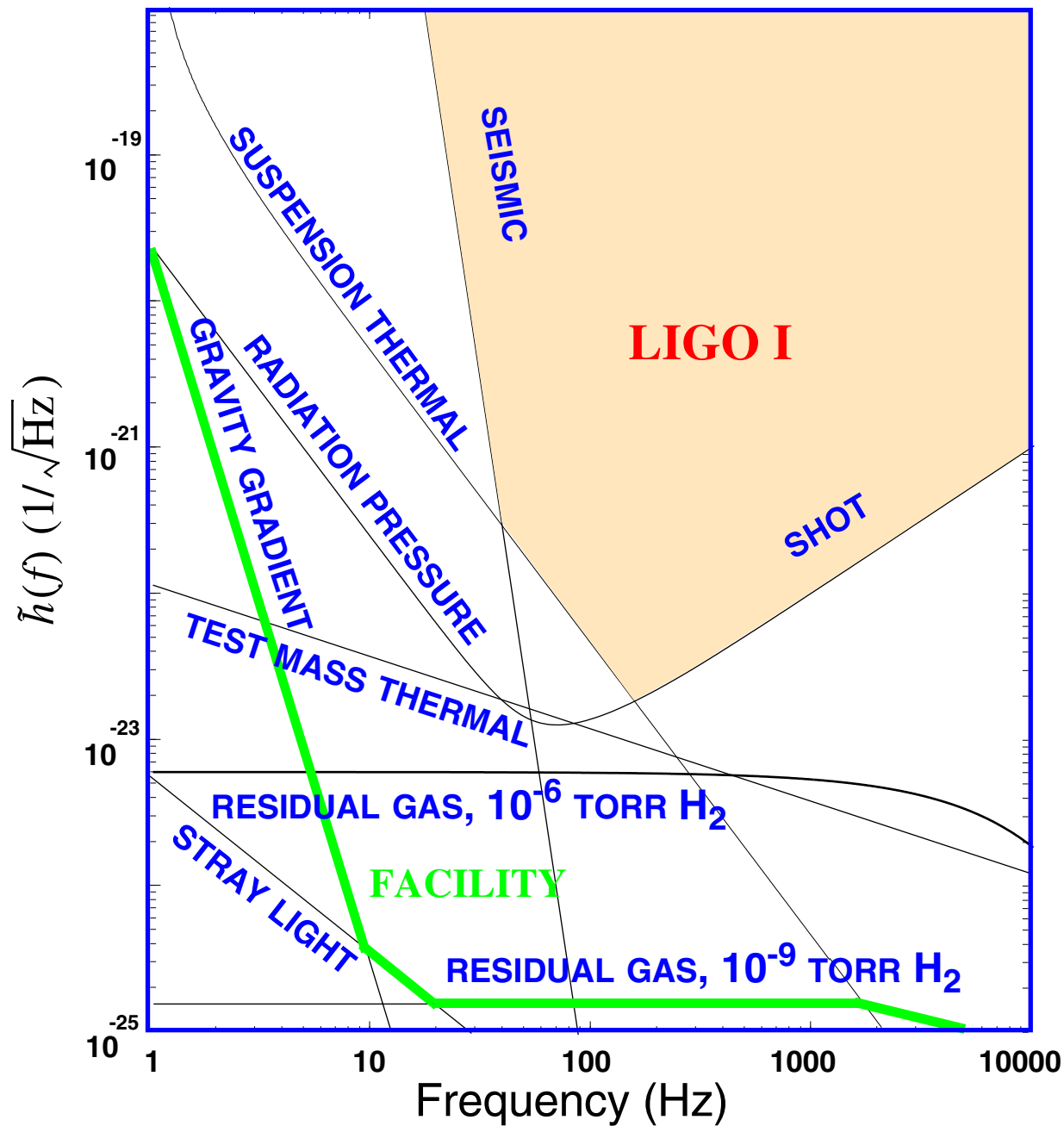
T_c = coherence or damping time
= $Q \times$ period of oscillator

Exchange with surroundings:

$$E(\text{thermal}) = \frac{kT}{T_c}$$

Large $T_c \Rightarrow$ smaller fluctuations

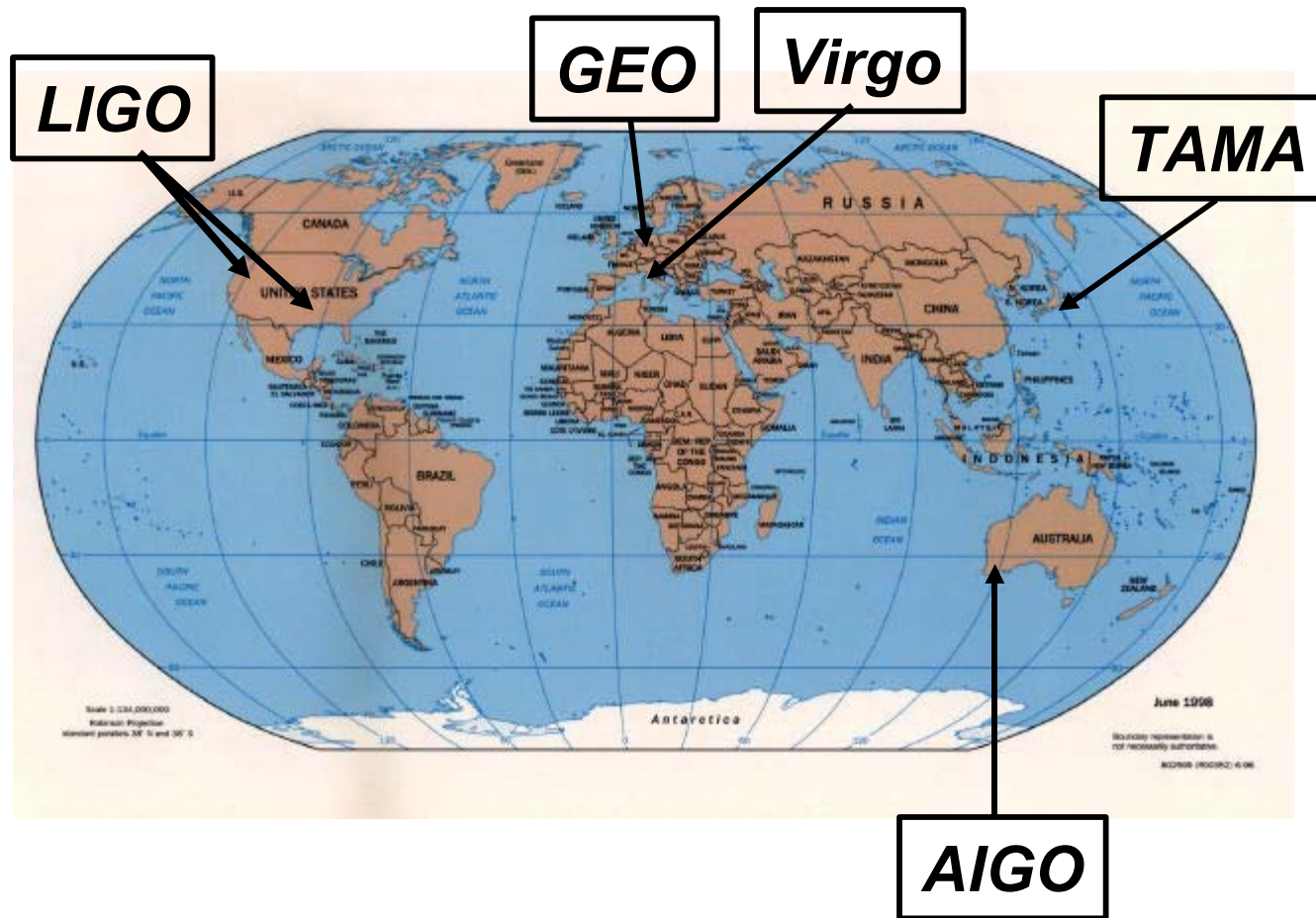




Interferometers

international network

Simultaneously detect signal (within msec)



detection
confidence

locate the
sources

decompose the
polarization of
gravitational
waves



LIGO Observatory Facilities



LIGO Hanford Observatory [LHO]

26 km north of Richland, WA

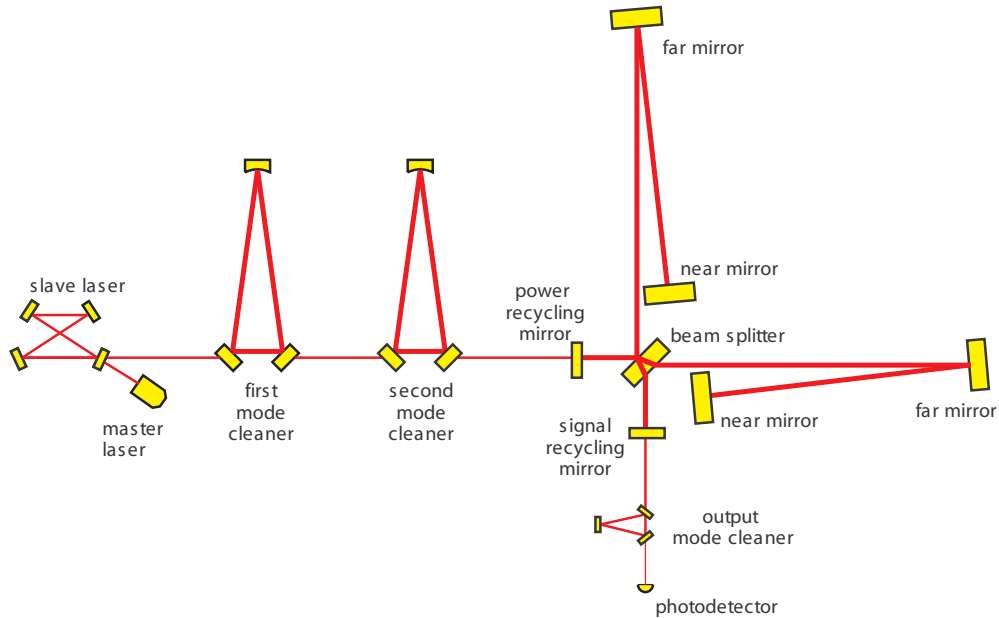
2 km + 4 km interferometers in same vacuum envelope



LIGO Livingston Observatory [LLO]

42 km east of Baton Rouge, LA

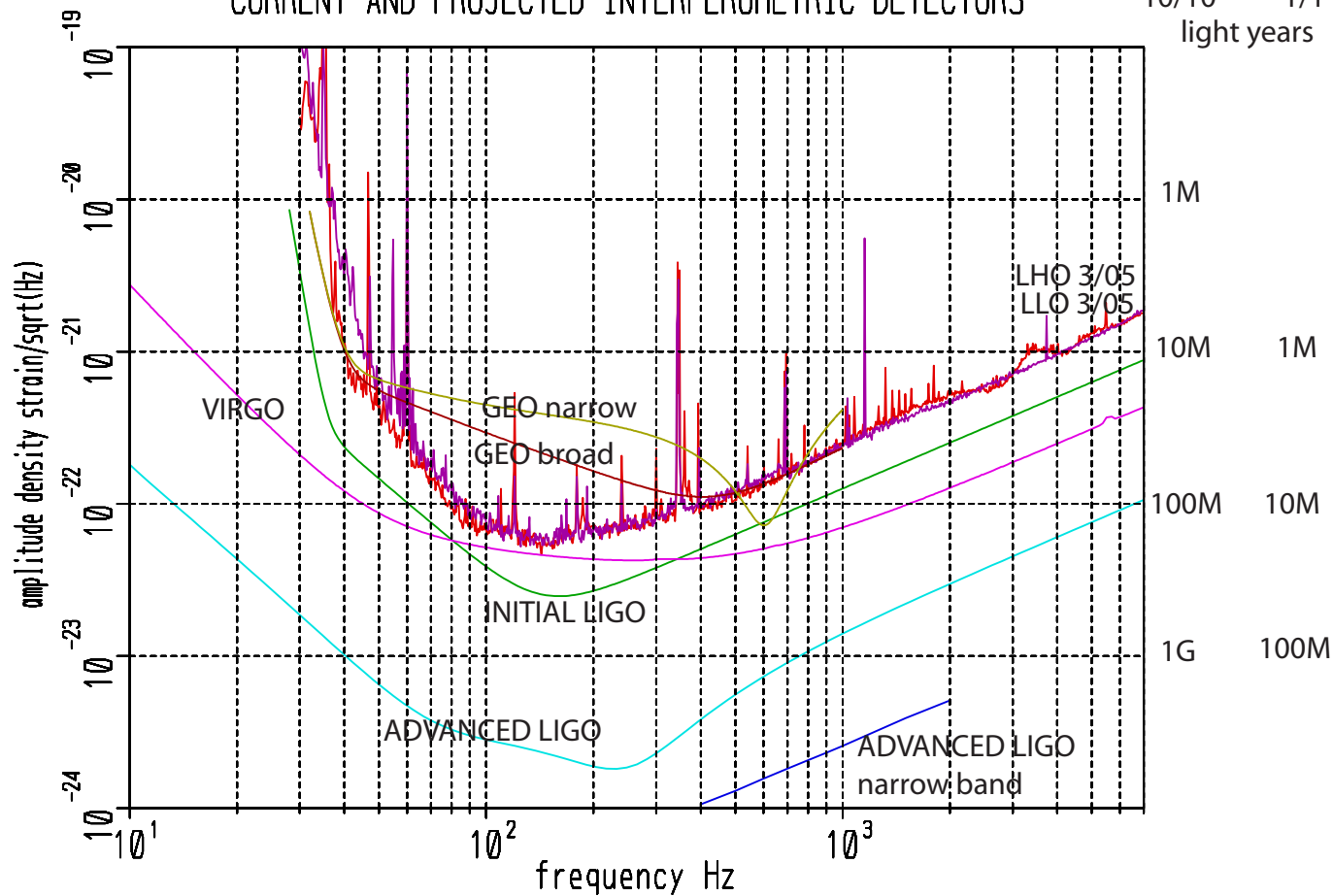
Single 4 km interferometer



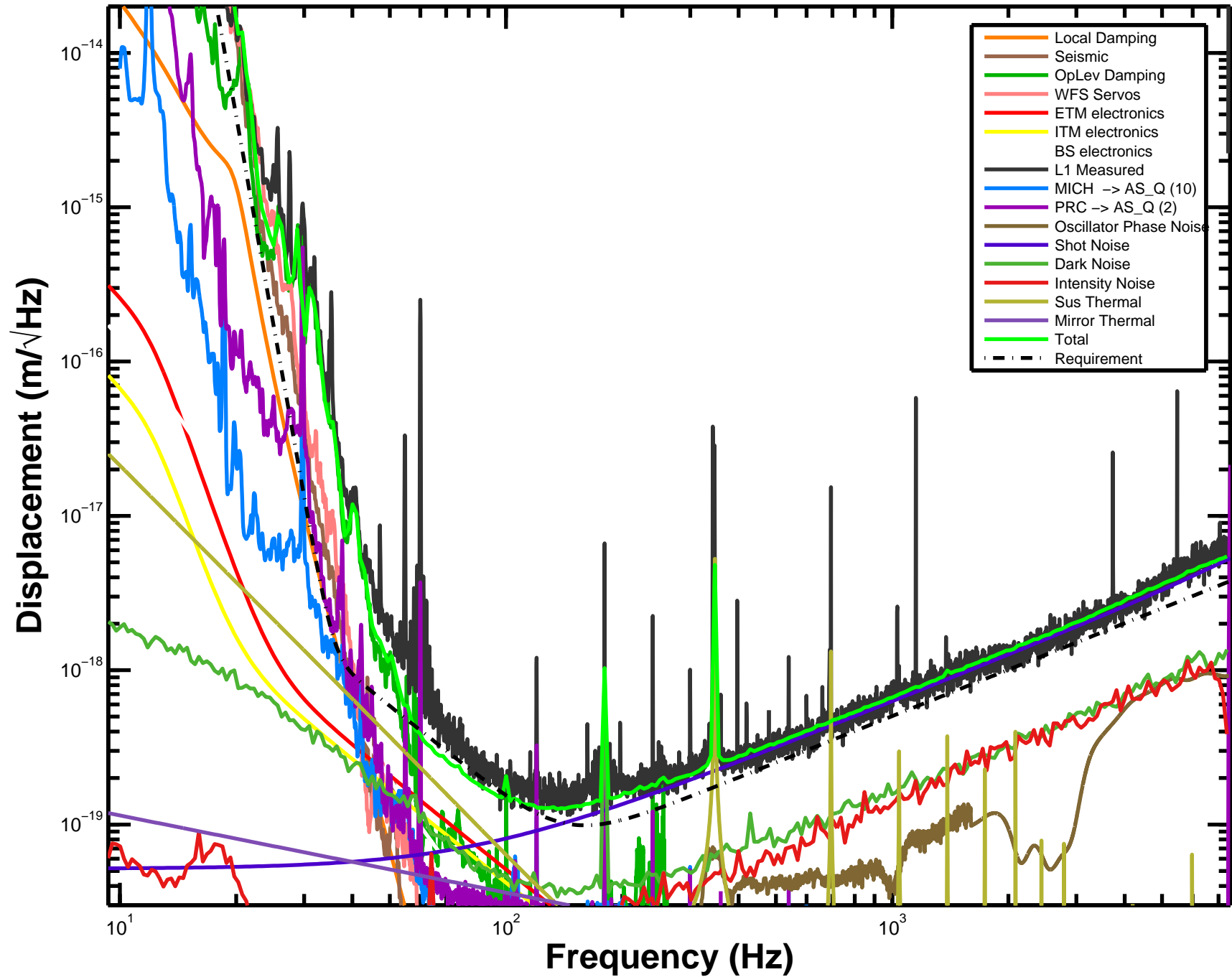


CURRENT AND PROJECTED INTERFEROMETRIC DETECTORS

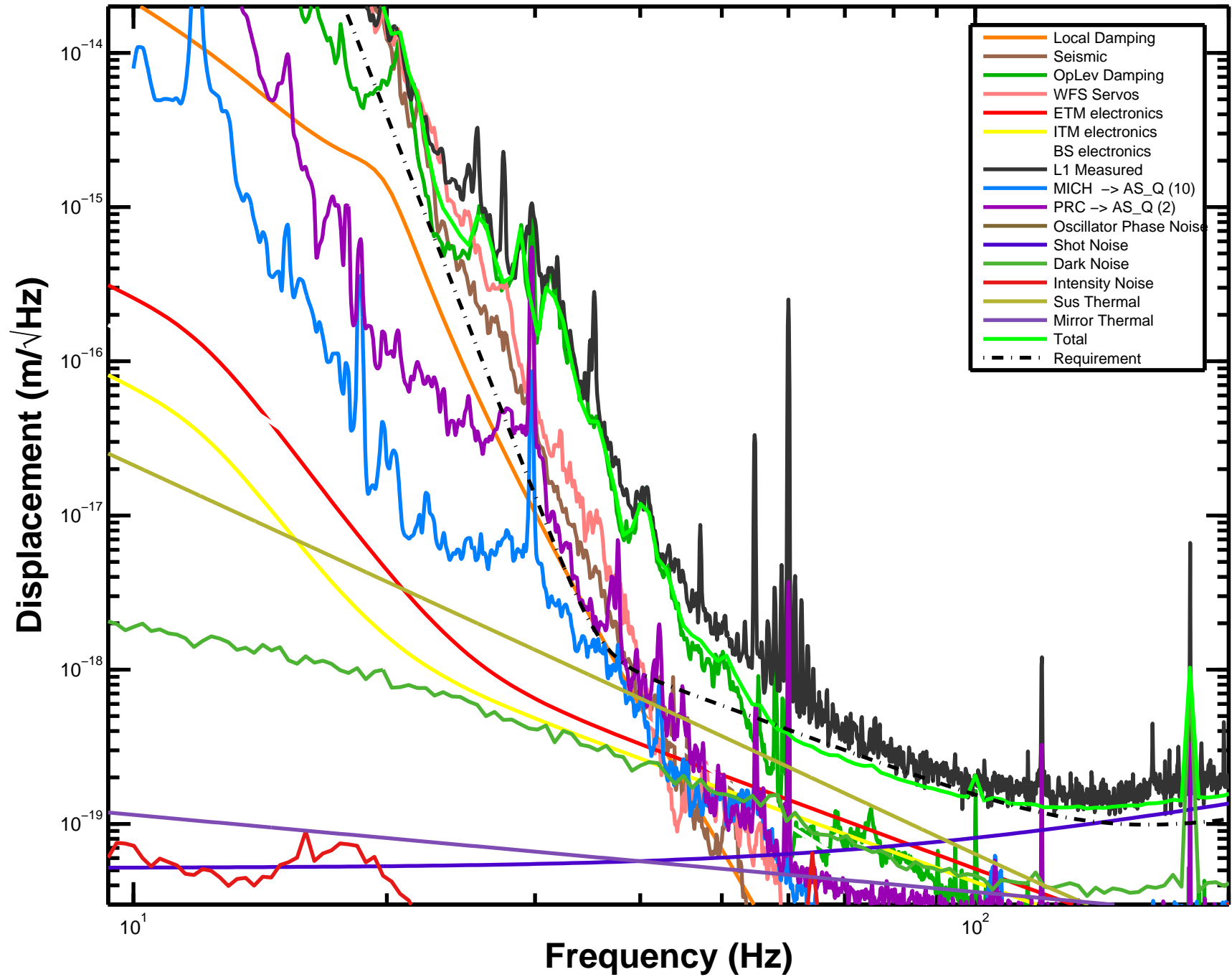
BH/BH NS/NS
10/10 1/1
light years



L1: 10.1 Mpc, Apr 20 2005 06:01:38 UTC



L1: 10.1 Mpc, Apr 20 2005 06:01:38 UTC



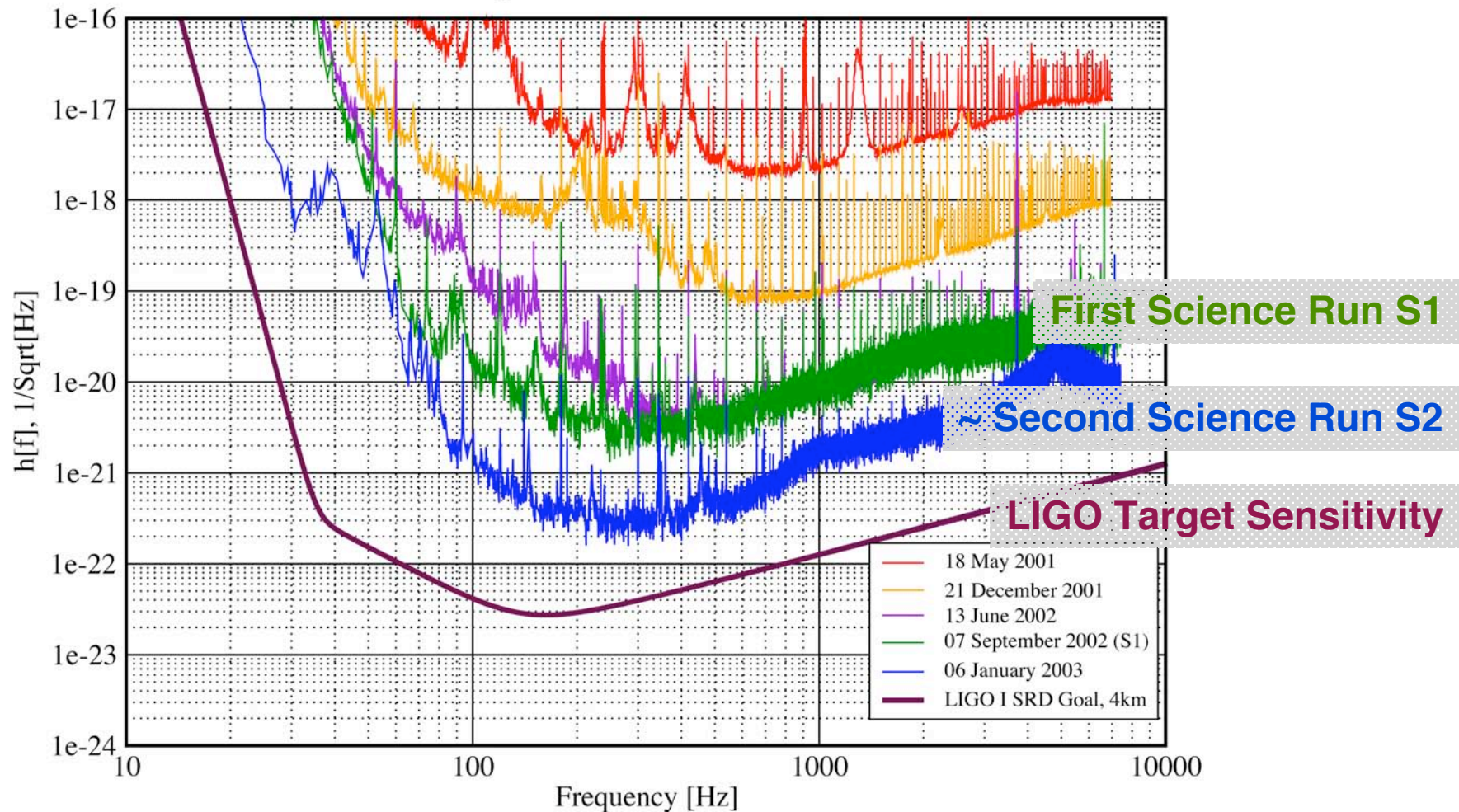


Gravitational Radiation and Detectors: LIGO Sensitivity Improvements

Strain Sensitivity for the LLO 4km Interferometer

31 January 2003

LIGO-G030014-00-E



Classes of sources

- Compact binary inspiral: template search
 - BH/BH
 - NS/NS and BH/NS
- Low duty cycle transients: wavelets, T/f clusters
 - Supernova
 - BH normal modes
 - Unknown types of sources
- Periodic CW sources
 - Pulsars
 - Low mass x-ray binaries (quasi periodic)
- Stochastic background
 - Foreground sources : gravitational wave radiometry
 - Cosmological isotropic background

Rate < 47 inspirals/yr/milky way galaxy to a distance of 1.5Mpc
 Mass range 1 to 3 solar masses

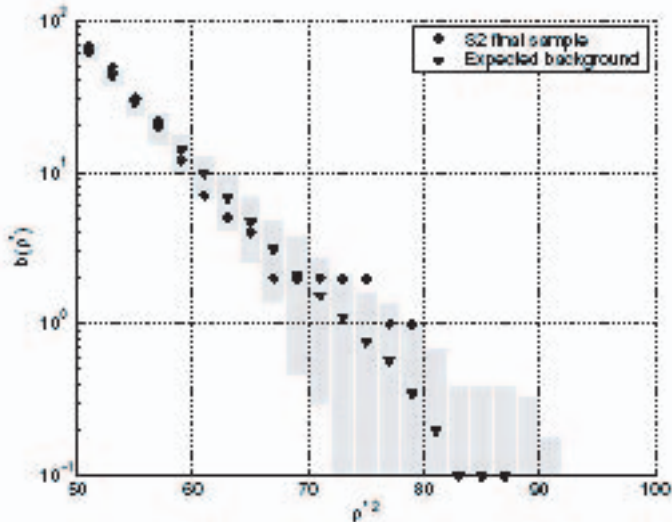


FIG. 10: The mean number of triggers per S2 above SNR ρ^* using the best fit clustering method. The triangles represent the expected background. See Fig. 8 and Sec. VII for details of the time-shifts and for comparison with largest SNR clustering. We note that there is no apparent excess of S2 coincident triggers over the expected background from accidental coincidences in this plot.

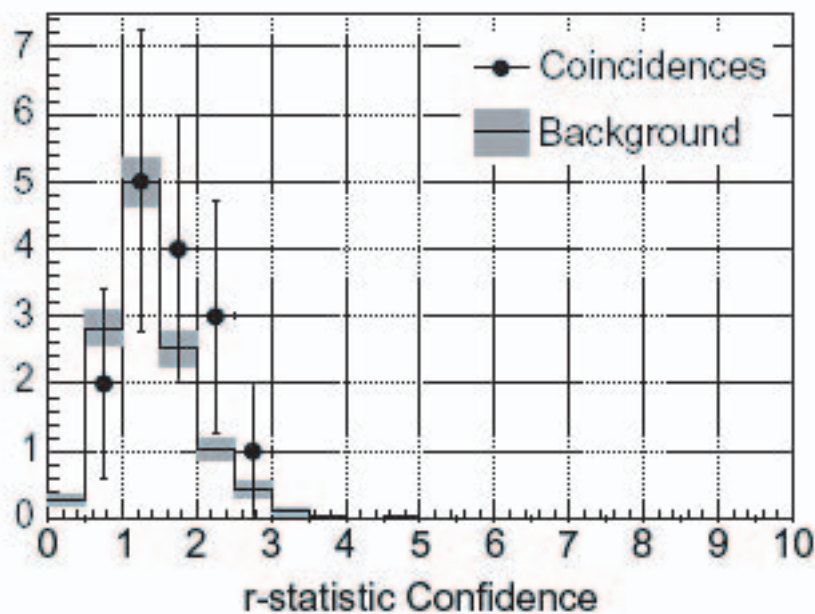


FIG. 7: Histogram of r -statistic confidence values (Γ 's), for events passing the WaveBurst analysis at zero-lag (shown with circles) and at time-shifts (*i.e.*, background, shown with bars), after applying the acoustic veto. The histogram of background events is normalized to the live-time of the zero-lag analysis.

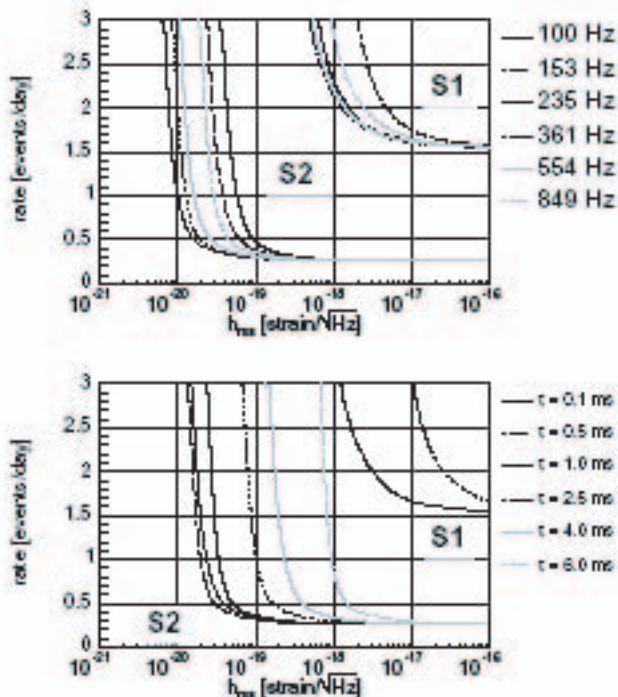


FIG. 12: Rate versus h_{rms} exclusion plots at the 90% confidence level derived from the LIGO burst search using the S2 data. The top plot corresponds to burst events modeled by sine-Gaussians of $Q = 8.9$ and frequencies ranging from 100 Hz to 850 Hz, while the bottom plot corresponds to ones events modeled by Gaussians of the τ 's shown. For comparison, the corresponding curves resulting from the S1 analysis are superimposed.

pulsar	spin f (Hz)	spindown \dot{f} (Hz s $^{-1}$)	$h_0^{95\%}$ /10 $^{-24}$	ϵ /10 $^{-5}$
B0021-72C*	173.71	$+1.50 \times 10^{-15}$	4.3	16
B0021-72D*	186.65	$+1.19 \times 10^{-16}$	4.1	14
B0021-72F*	381.16	-9.37×10^{-15}	7.2	5.7
B0021-72G*	247.50	$+2.58 \times 10^{-15}$	4.1	7.5
B0021-72L*	230.09	$+6.46 \times 10^{-15}$	2.9	6.1
B0021-72M*	271.99	$+2.84 \times 10^{-15}$	3.3	5.0
B0021-72N*	327.44	$+2.34 \times 10^{-15}$	4.0	4.3
J0030+0451	205.53	-4.20×10^{-16}	3.8	0.48
B0531+21*	29.81	-3.74×10^{-10}	41	2 100
J0711-6830	182.12	-4.94×10^{-16}	2.4	1.8
J1024-0719*	193.72	-6.95×10^{-16}	3.9	0.86
B1516+02A	180.06	-1.34×10^{-15}	3.6	21
J1629-6902	166.65	-2.78×10^{-16}	2.3	2.7
J1721-2457	285.99	-4.80×10^{-16}	4.0	1.8
J1730-2304*	123.11	-3.06×10^{-16}	3.1	2.5
J1744-1134*	245.43	-5.40×10^{-16}	5.9	0.83
J1748-2446C	118.54	$+8.52 \times 10^{-15}$	3.1	24
B1820-30A*	183.82	-1.14×10^{-13}	4.2	24
B1821-24*	327.41	-1.74×10^{-13}	5.6	7.1
J1910-5959B	119.65	$+1.14 \times 10^{-14}$	2.4	8.5
J1910-5959C	189.49	-7.90×10^{-17}	3.3	4.7
J1910-5959D	110.68	-1.18×10^{-14}	1.7	7.2
J1910-5959E	218.73	$+2.09 \times 10^{-14}$	7.5	7.9
J1913+1011*	27.85	-2.61×10^{-12}	51	6 900
J1939+2134*	641.93	-4.33×10^{-14}	13	2.7
B1951+32*	25.30	-3.74×10^{-12}	48	4 400
J2124-3358*	202.79	-8.45×10^{-16}	3.1	0.45
J2322+2057*	207.97	-4.20×10^{-16}	4.1	1.8

TABLE I: The 28 pulsars targeted in the S2 run, with approximate spin parameters. Pulsars for which radio timing data were taken over the S2 period are starred (*). The right-hand two columns show the 95% upper limit on h_0 , based on a coherent analysis using all the S2 data, and corresponding ellipticity values (ϵ , see text). These upper limit values do *not* include the uncertainties due to calibration and to pulsar timing accuracy, which are discussed in the text, nor uncertainties in the pulsar’s distance, r .

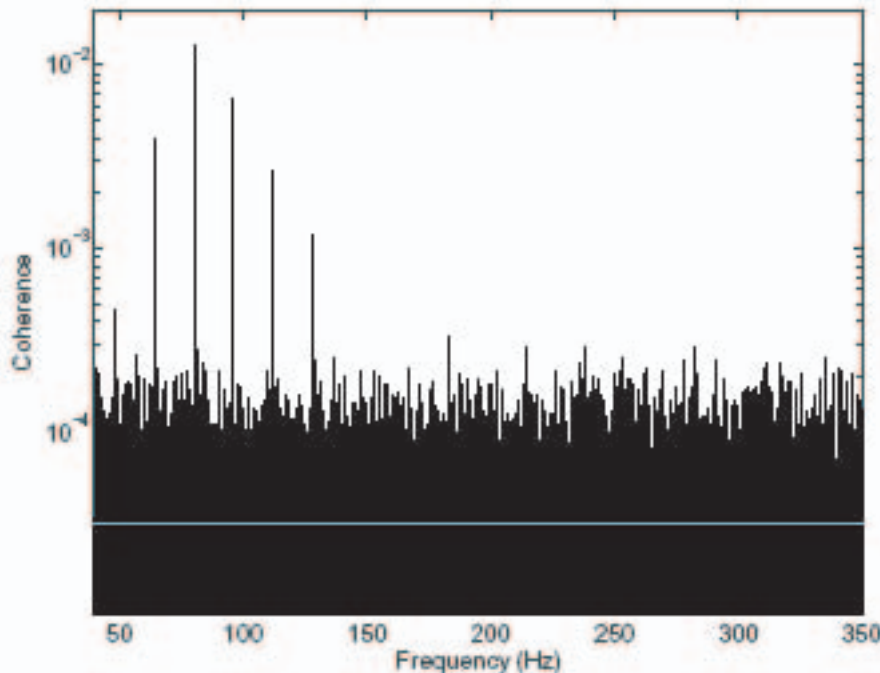
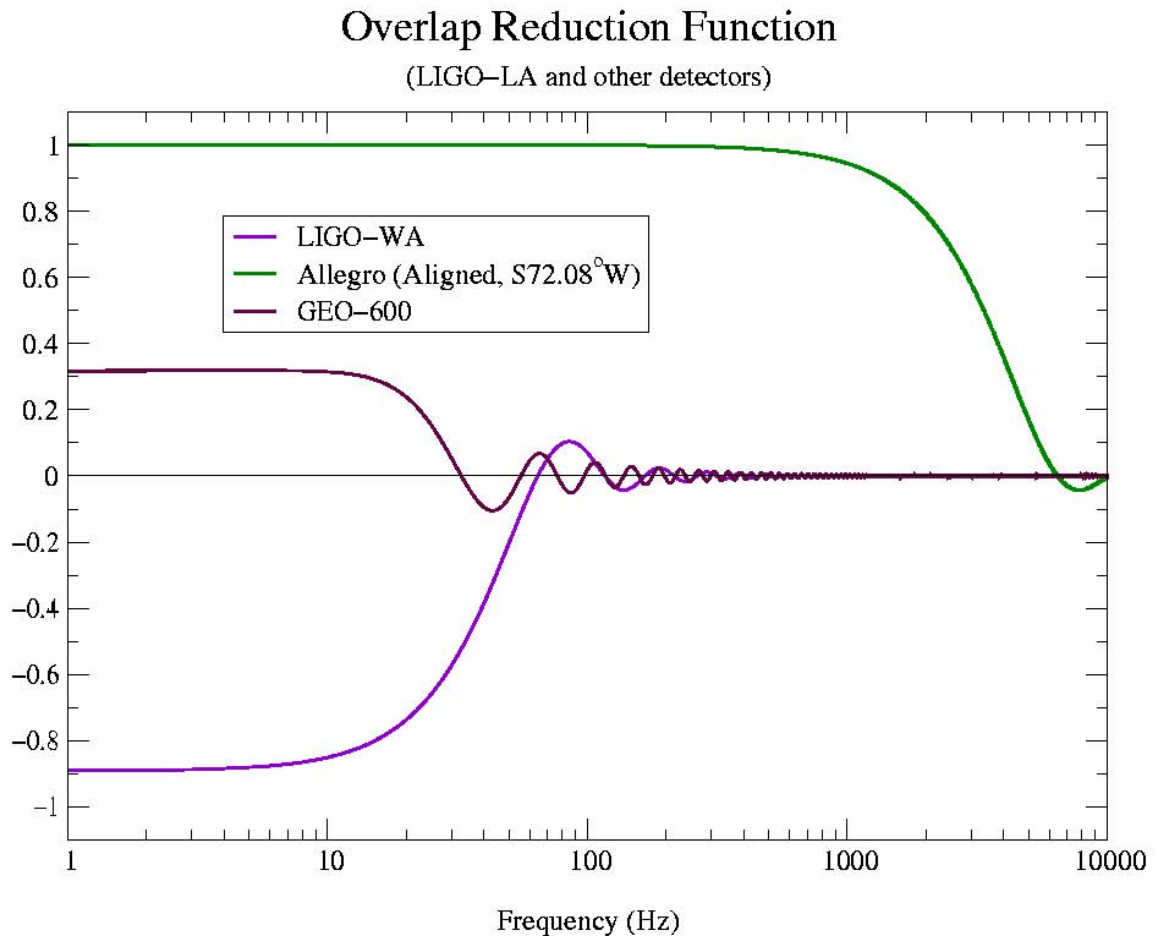
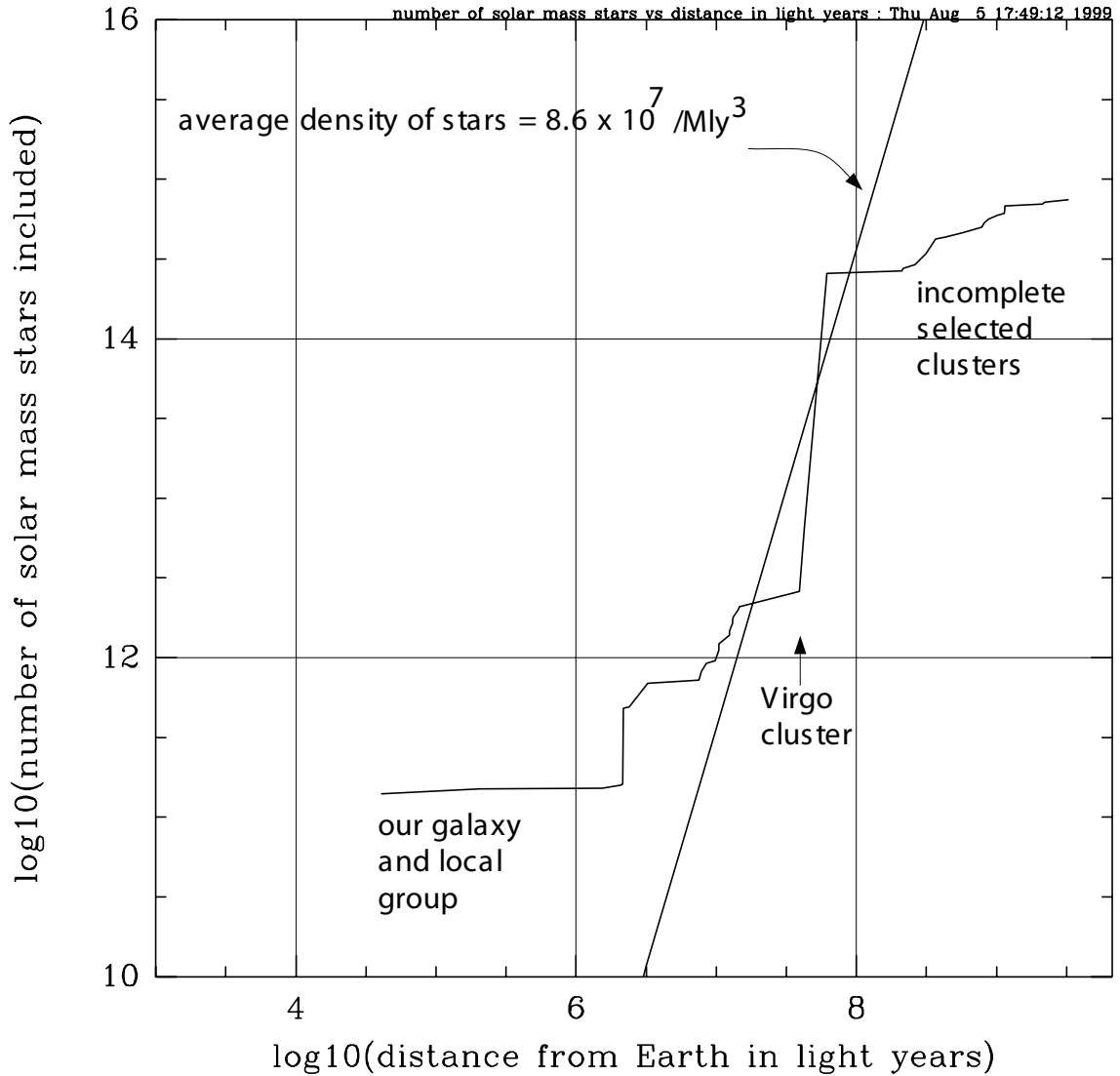


FIG. 2: Coherence between the H1 and L1 detector outputs during S3, showing a few small, but significant, coherent peaks at multiples of 16 Hz. The grey line corresponds to the expected statistical uncertainty level of $1/N_{\text{avg}} \approx 3 \times 10^{-5}$.

Overlap reduction function

Specifies the reduction in sensitivity due to the **separation** and **orientation** of the two detectors:





DATA: Cosmology of the Local Group G.Lake
Astrophysical Quantities C.W.Allen



Binary Coalescence Sources & Science: Binary Neutron Stars: S1 Range

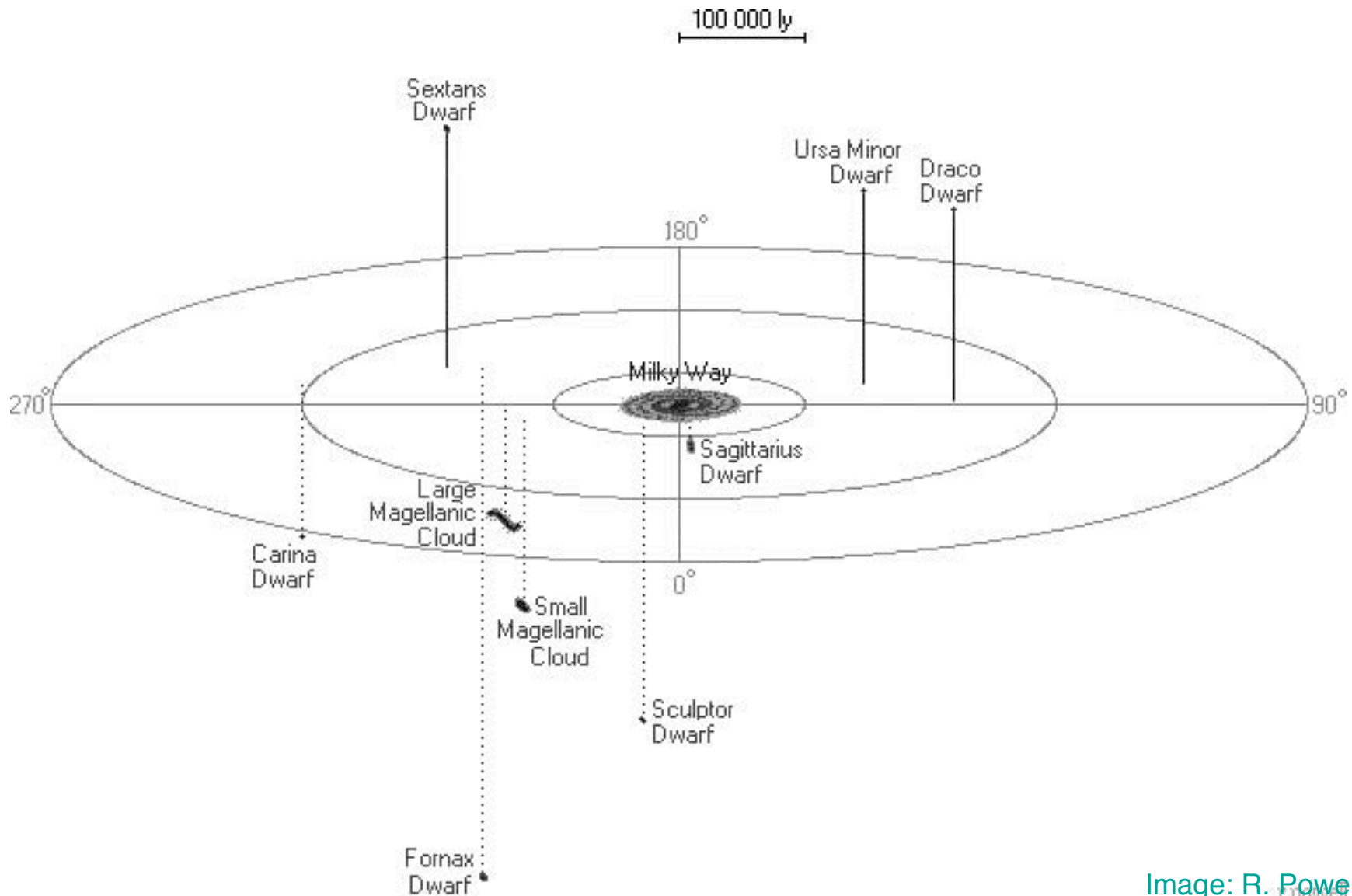


Image: R. Powell



Binary Coalescence Sources & Science: Binary Neutron Stars: S2 Range

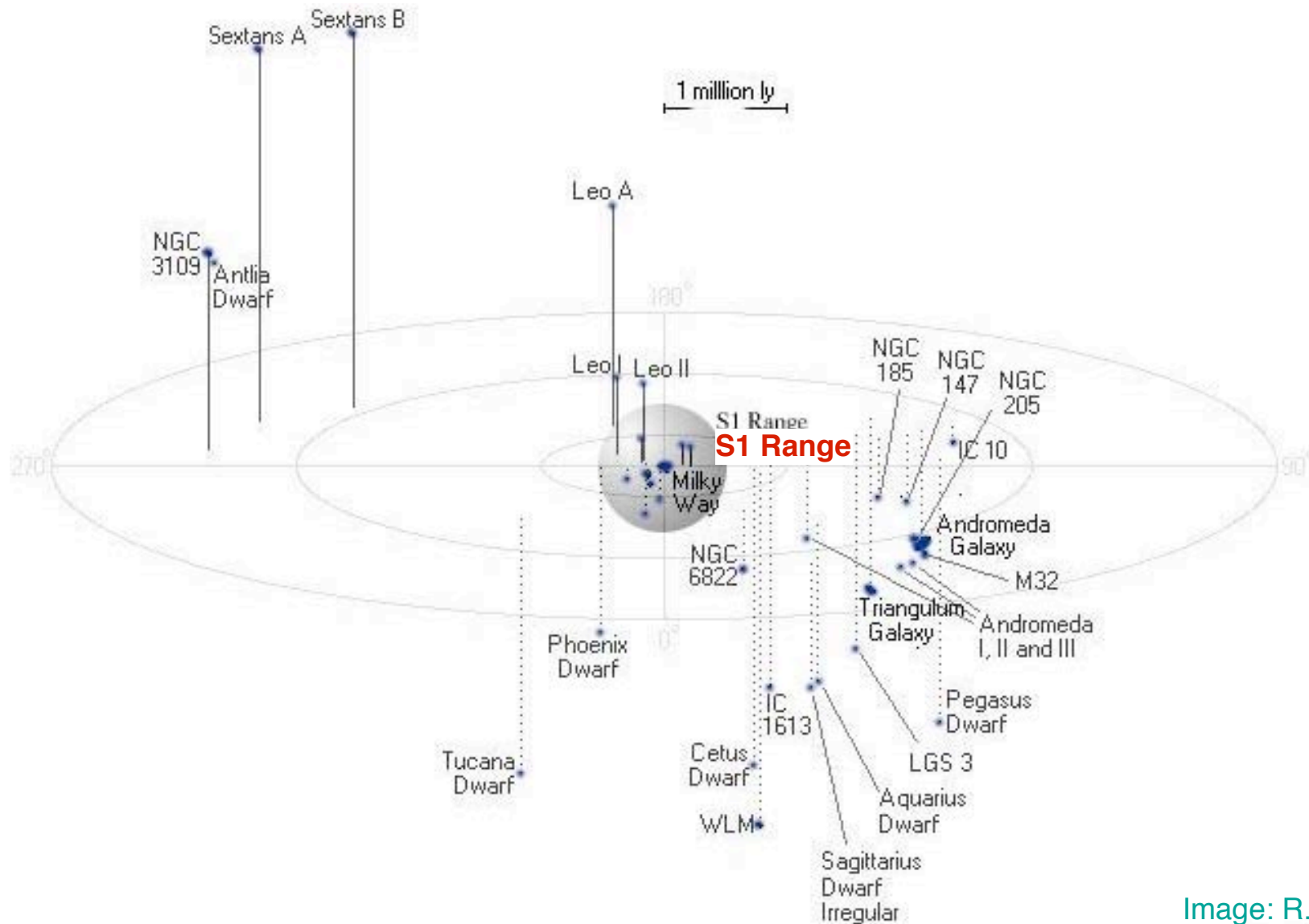


Image: R. Powell

cpowell



Binary Coalescence Sources & Science: Binary Neutron Stars: LIGO Range

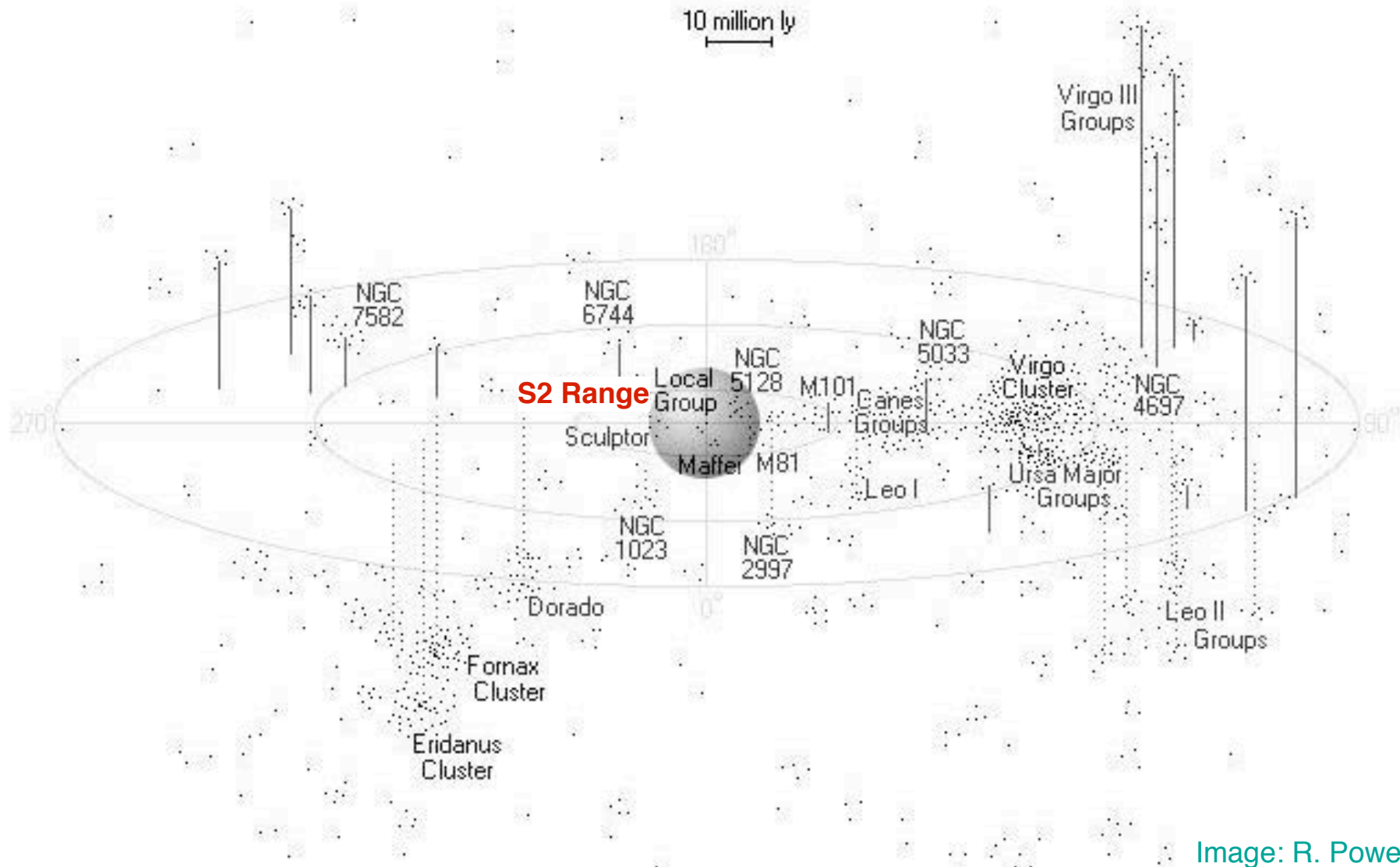
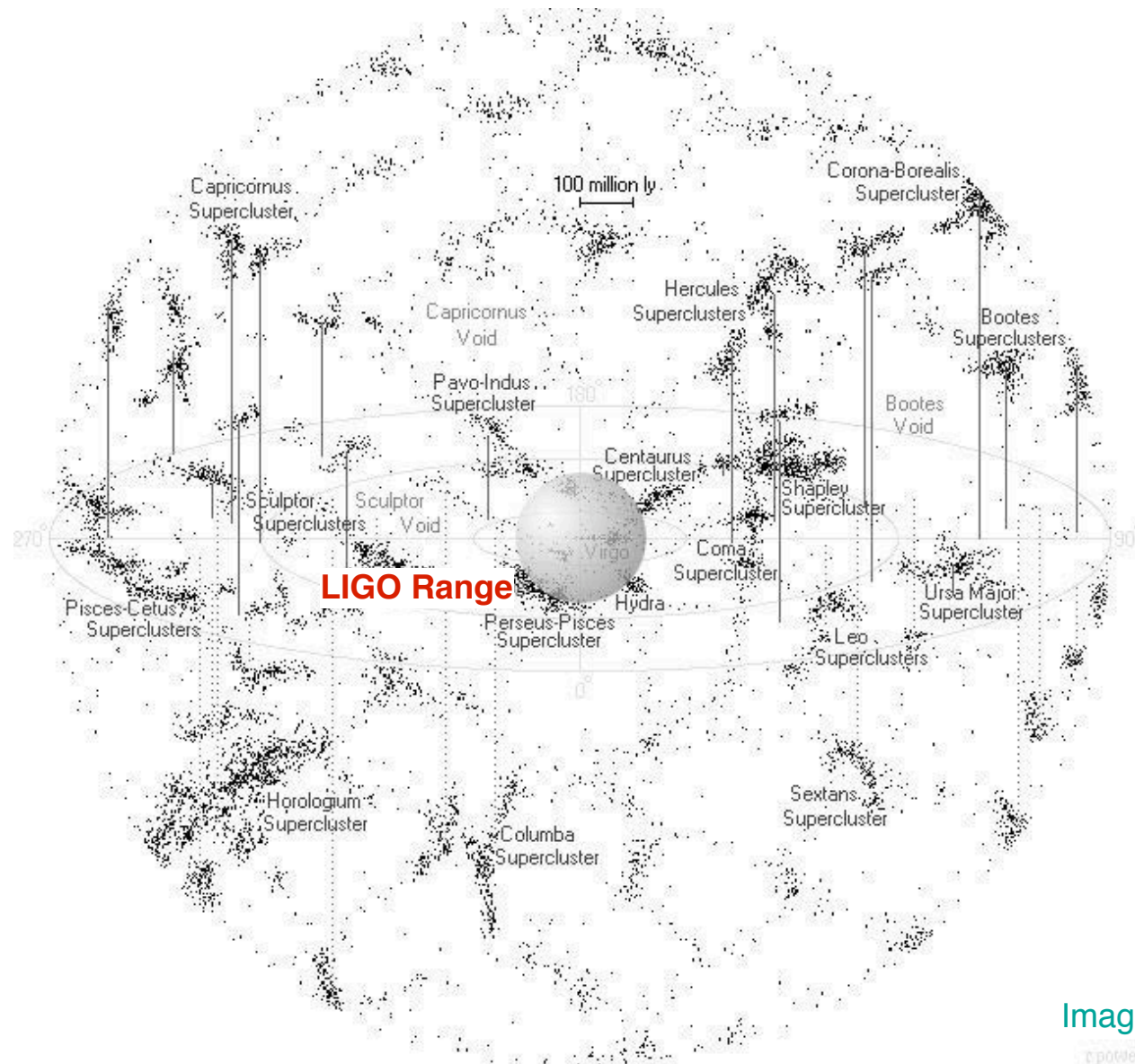


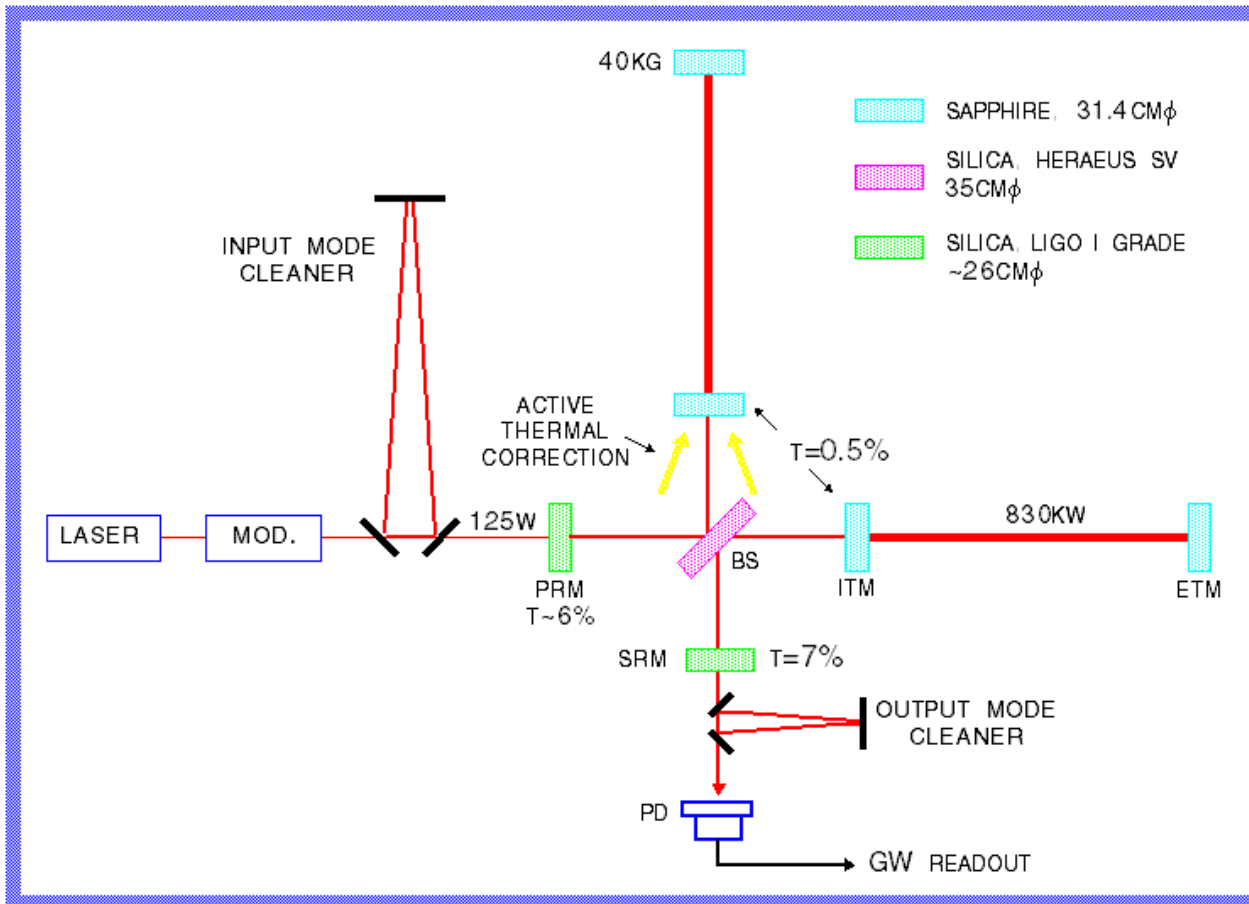
Image: R. Powell



Binary Coalescence Sources & Science: Binary Neutron Stars: AdLIGO Range



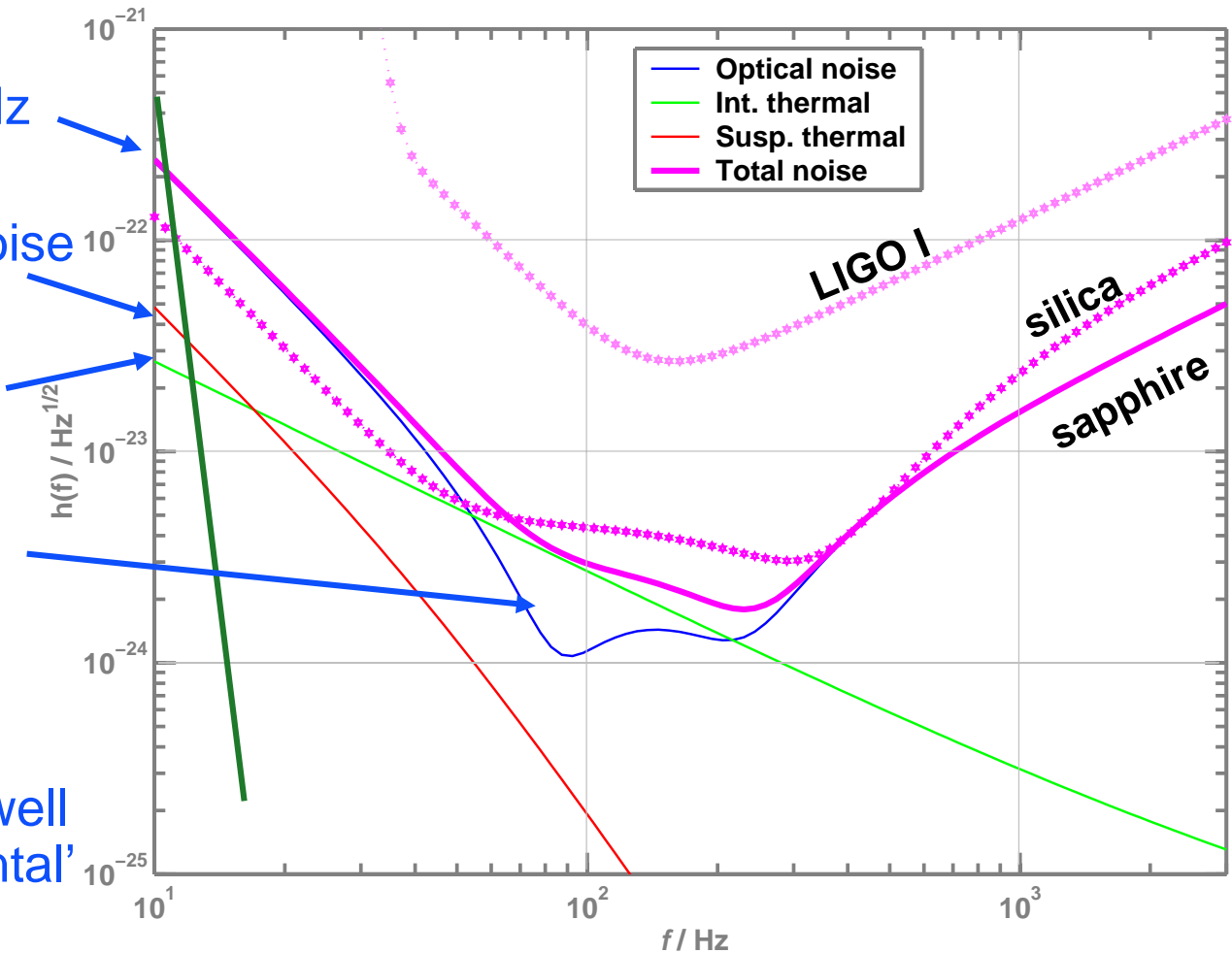
Advanced Interferometer Concept

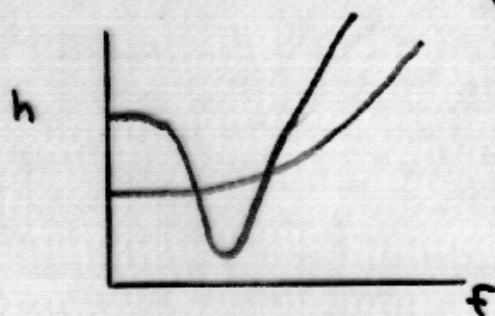
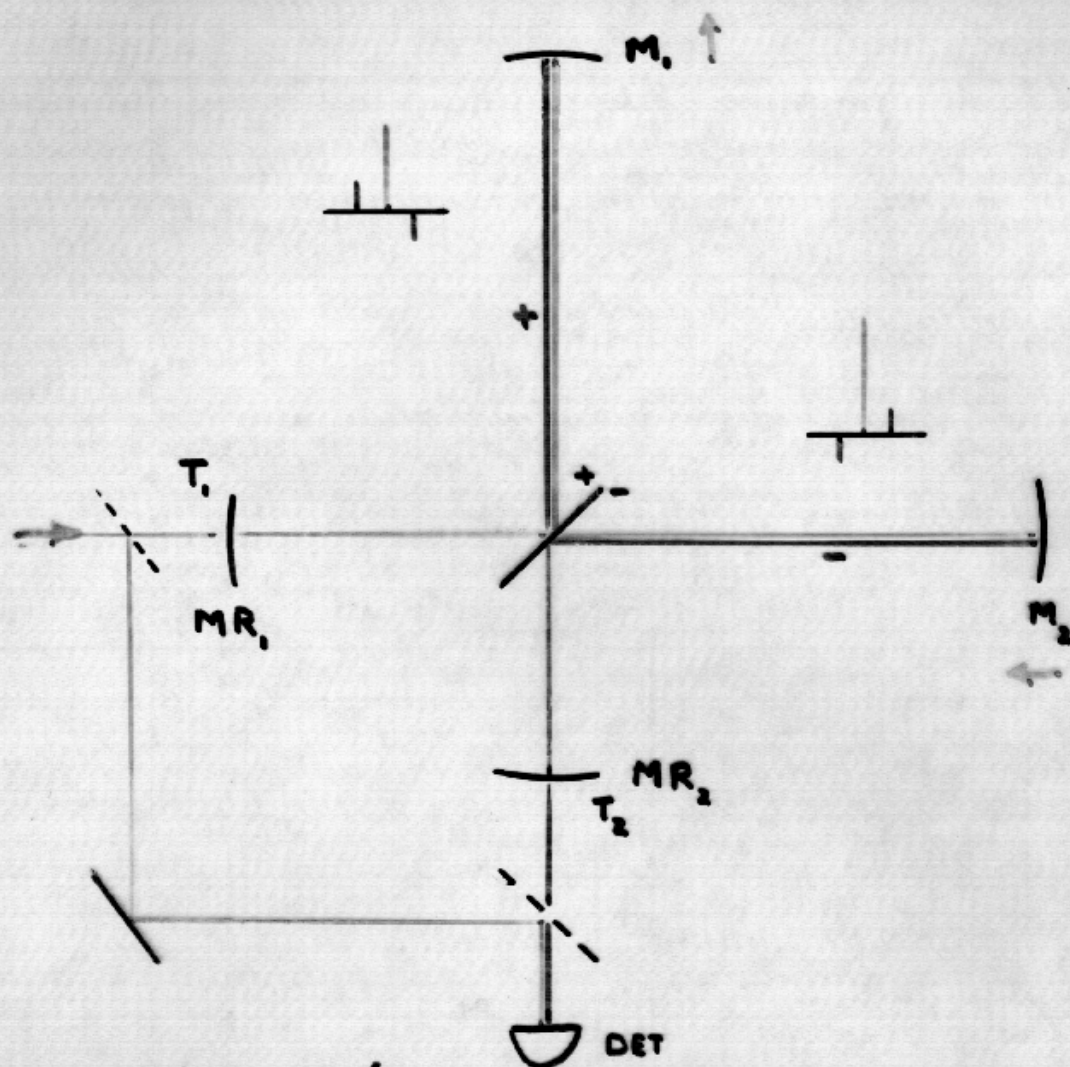


- » Signal recycling
- » 180-watt laser
- » 40 kg Sapphire test masses
- » Larger beam size
- » Quadruple suspensions
- » Active seismic isolation
- » Active thermal correction
- » Output mode cleaner

Projected Performance

- Seismic ‘cutoff’ at 10 Hz
- Suspension thermal noise
- Internal thermal noise
- Unified quantum noise dominates at most frequencies
- ‘technical’ noise (e.g., laser frequency) levels held in general well below these ‘fundamental’ noises



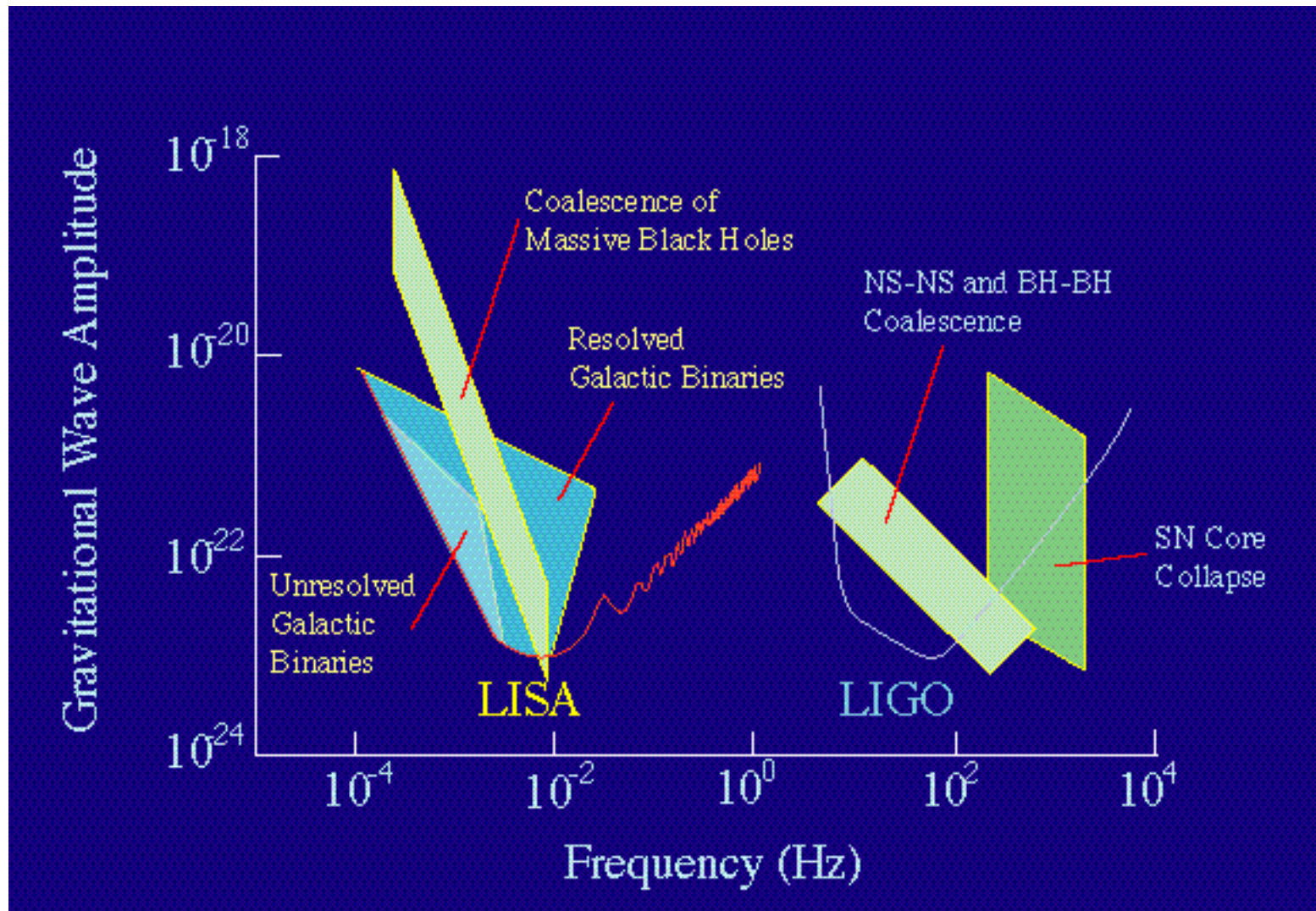


BRIAN MEERS

AMPLITUDE RECYCLED INTERFEROMETER

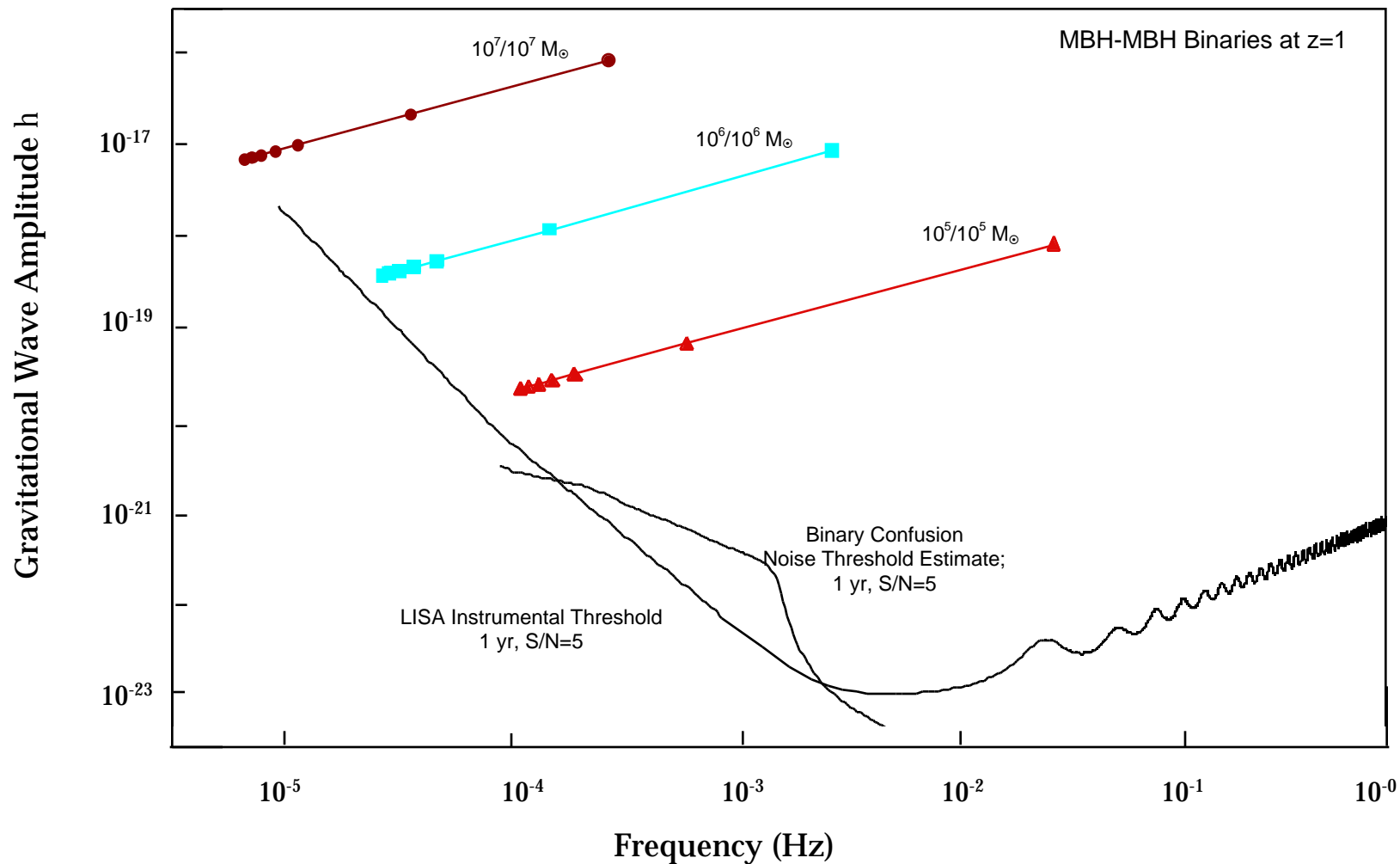


The Gravitational-Wave Spectrum



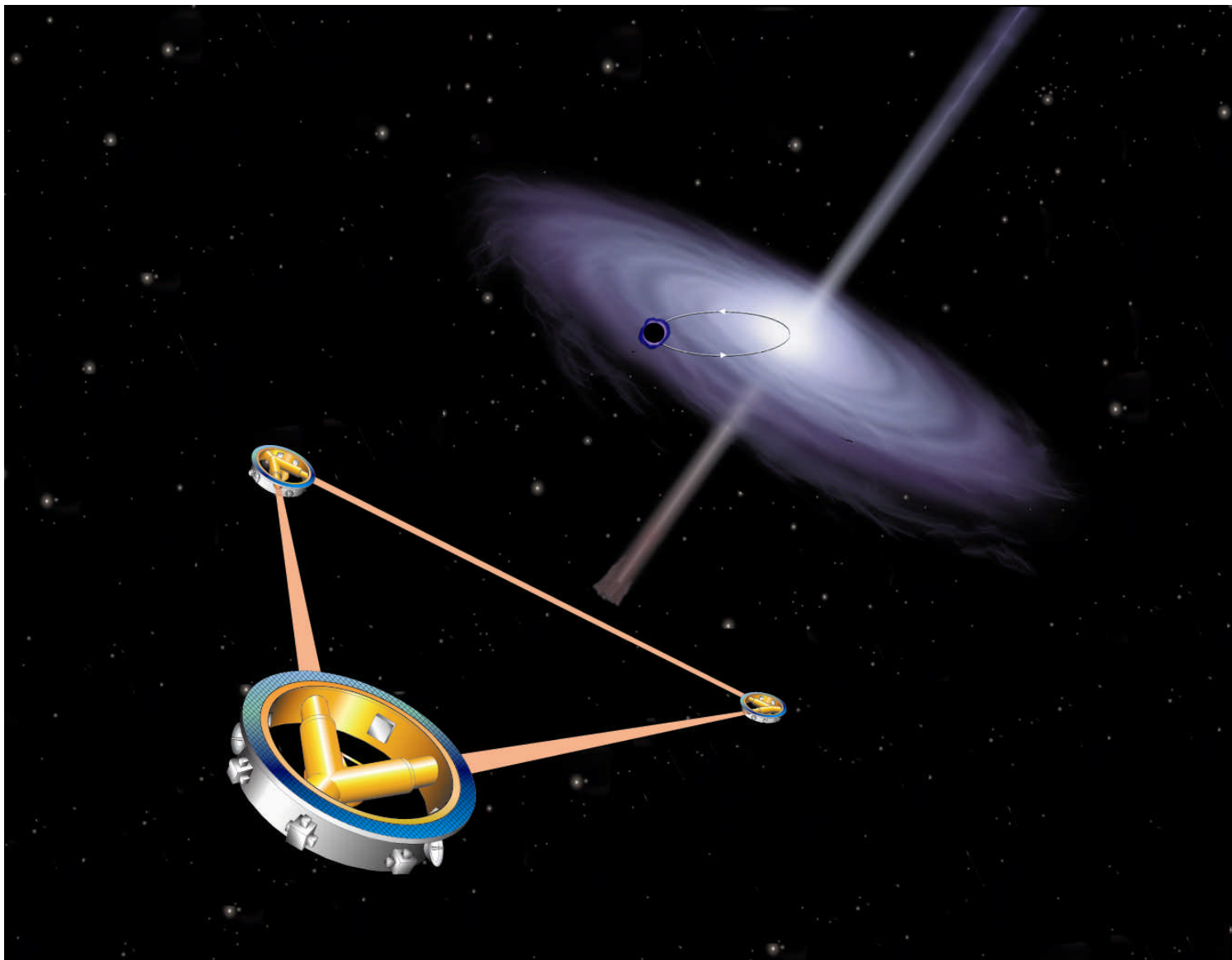


Massive Black Holes in Merging Galaxies





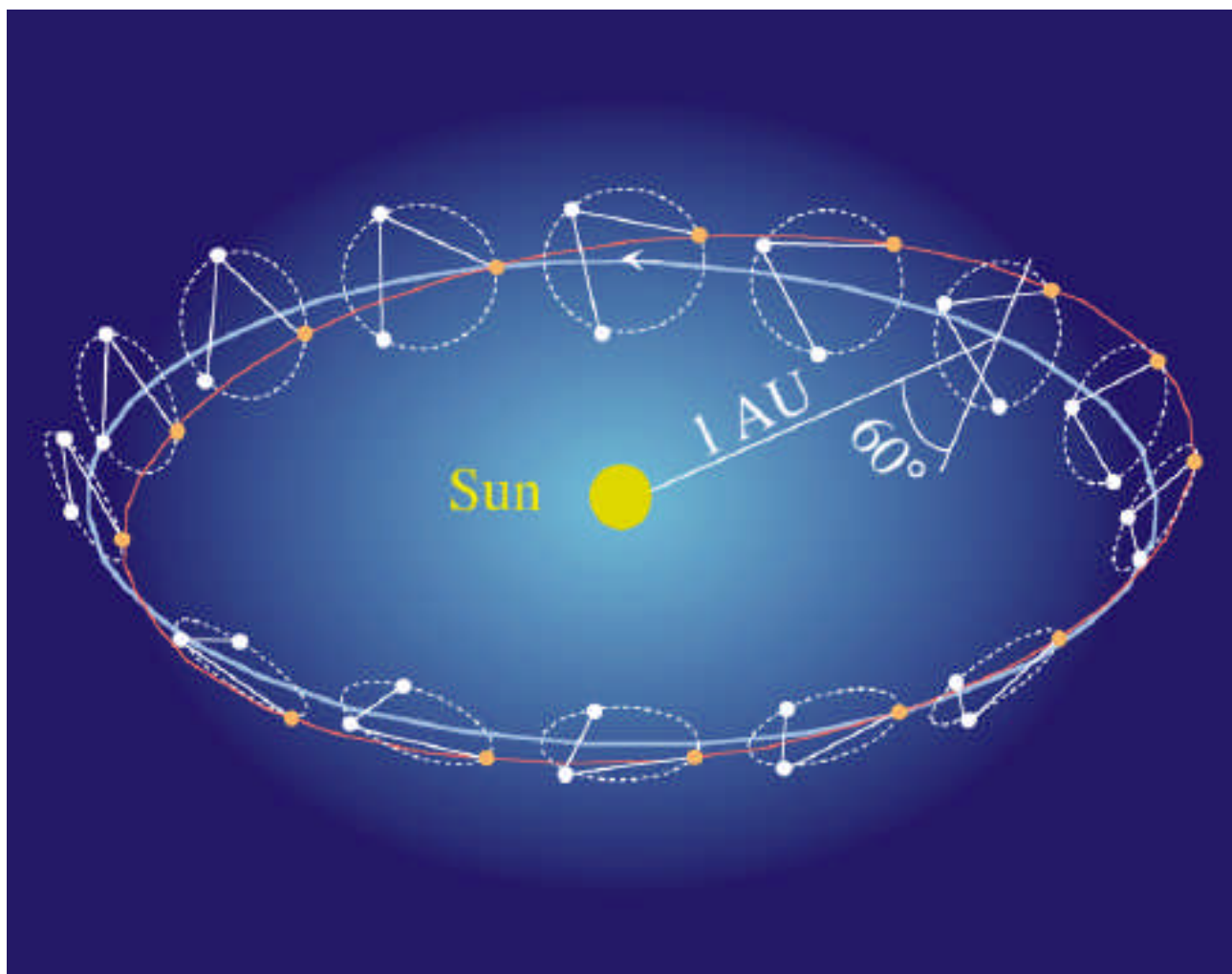
Mission Concept





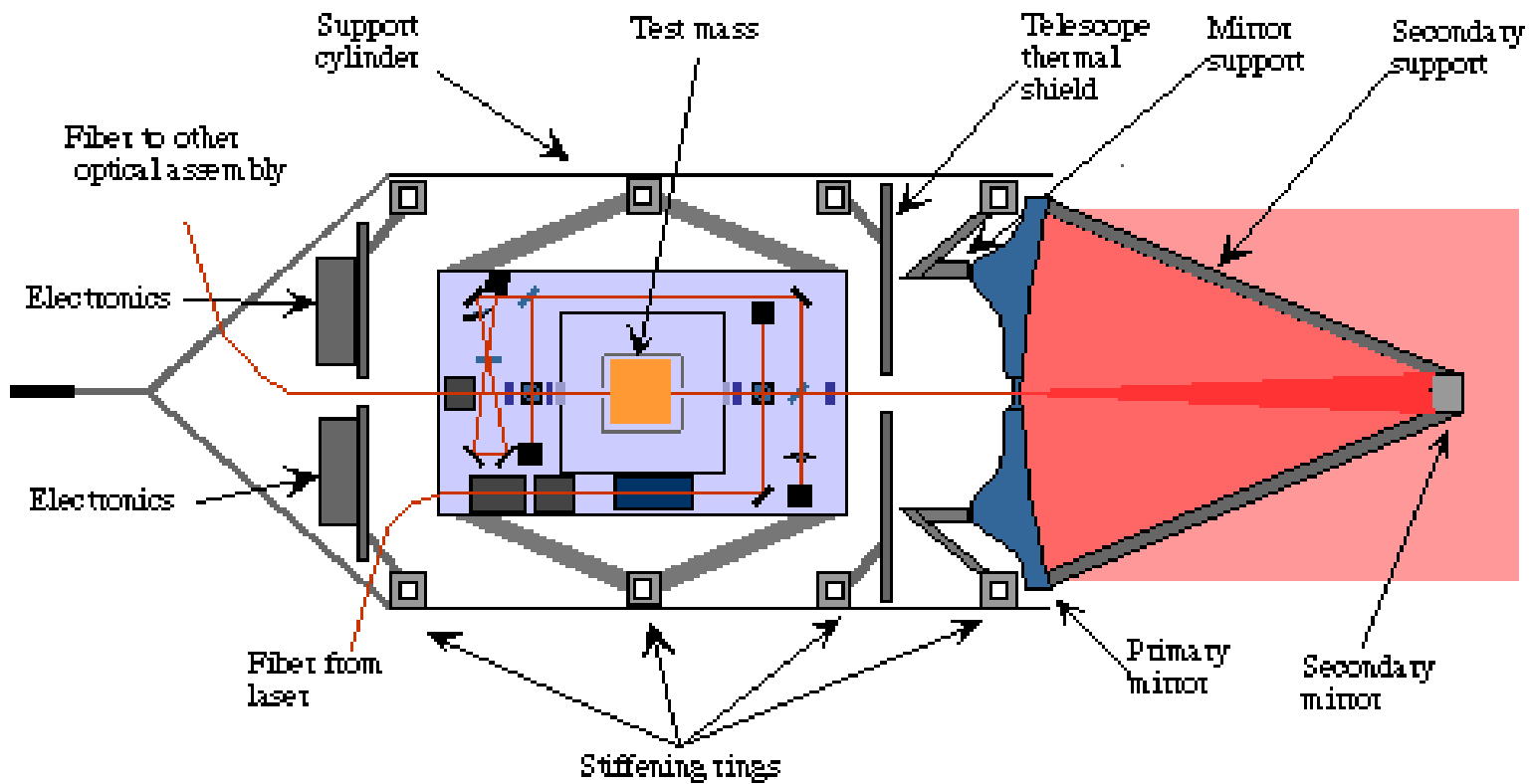
Spacecraft Orbits

- Spacecraft orbits evolve under gravitational forces only
- Spacecraft fly “drag-free” to shield proof masses from non-gravitational forces





Optical System



INFLATION

fraction
of a second

**CMB
last scattering**

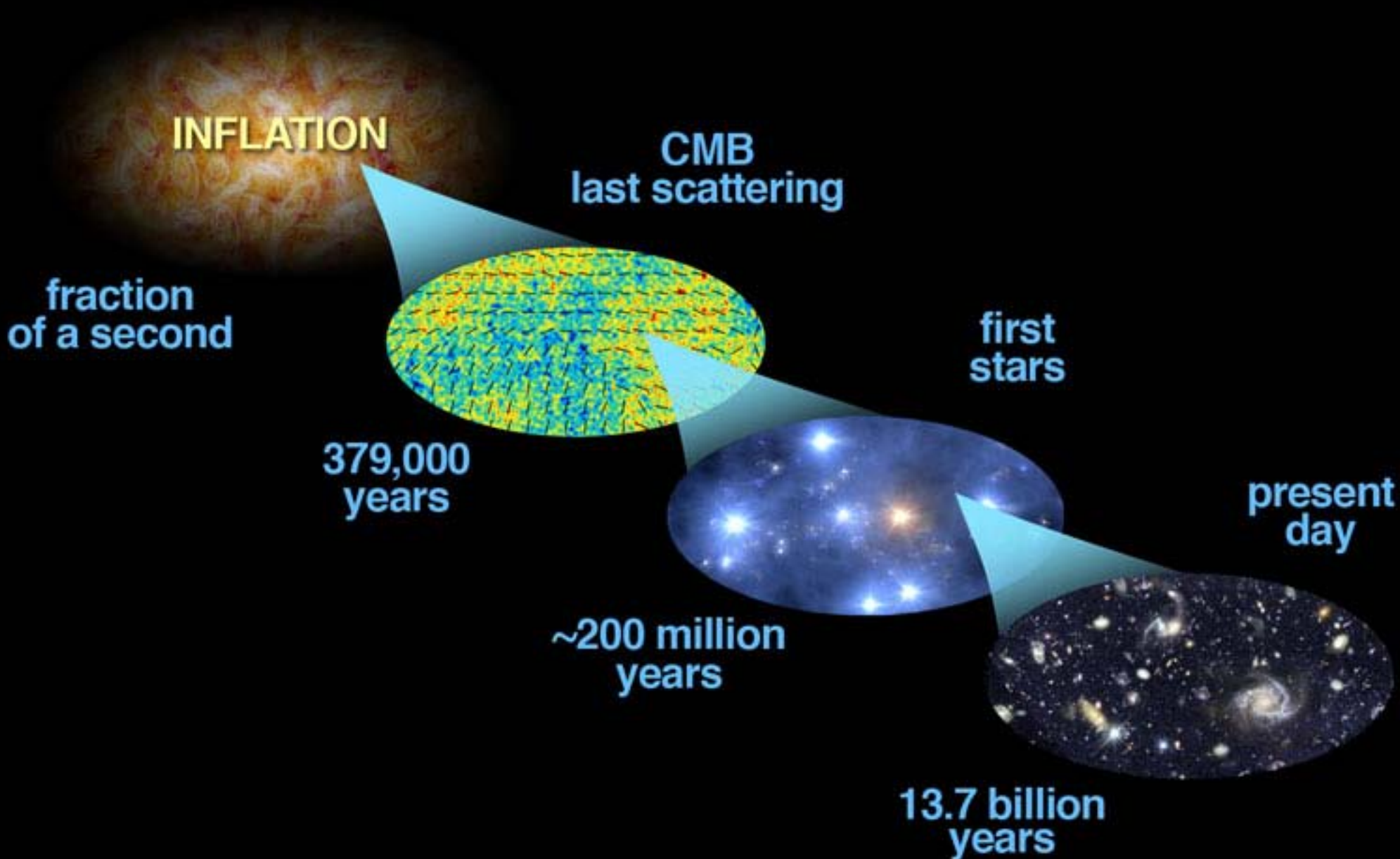
379,000
years

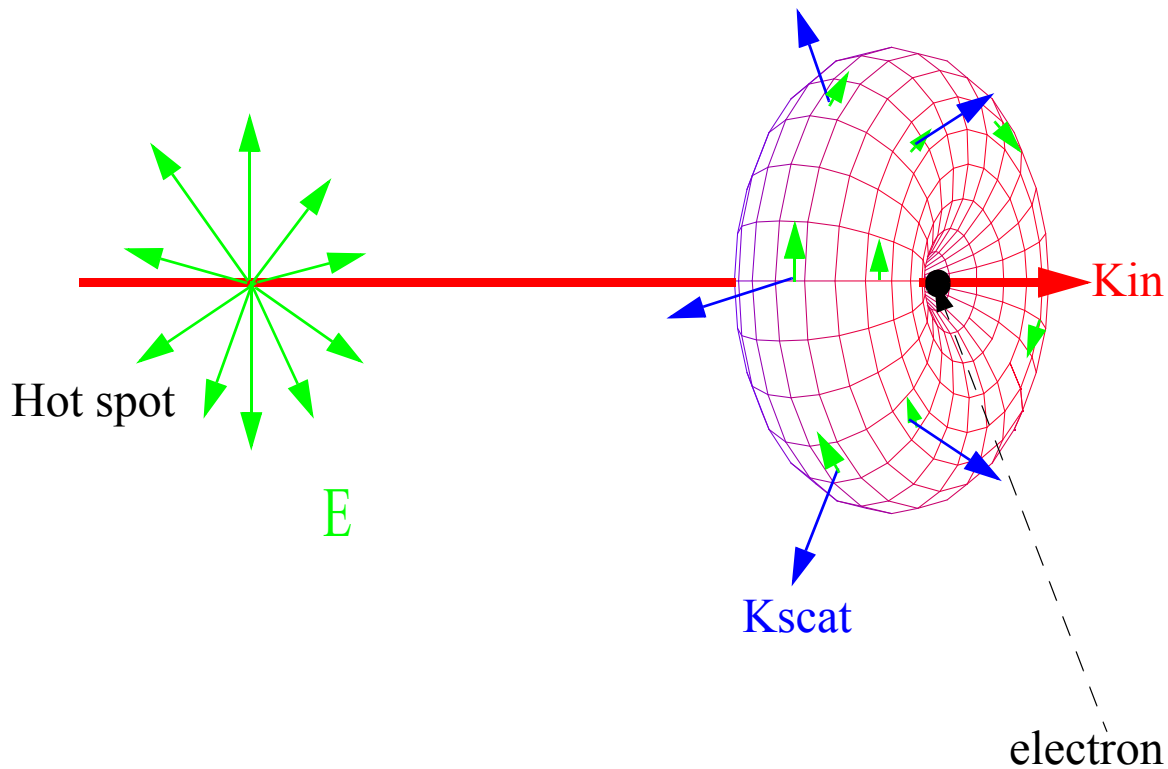
first
stars

~200 million
years

present
day

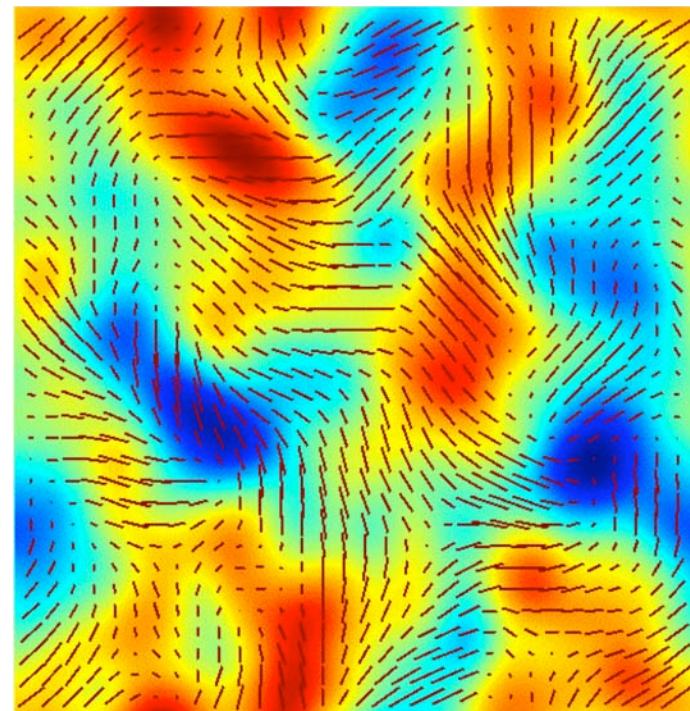
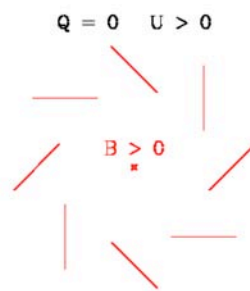
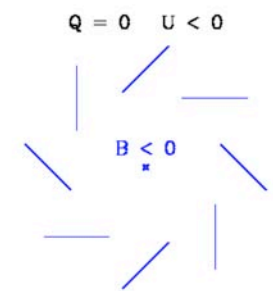
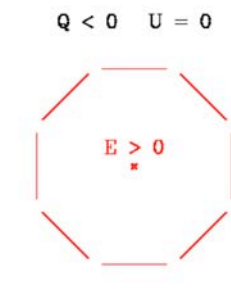
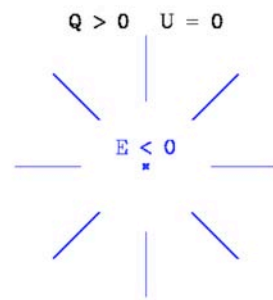
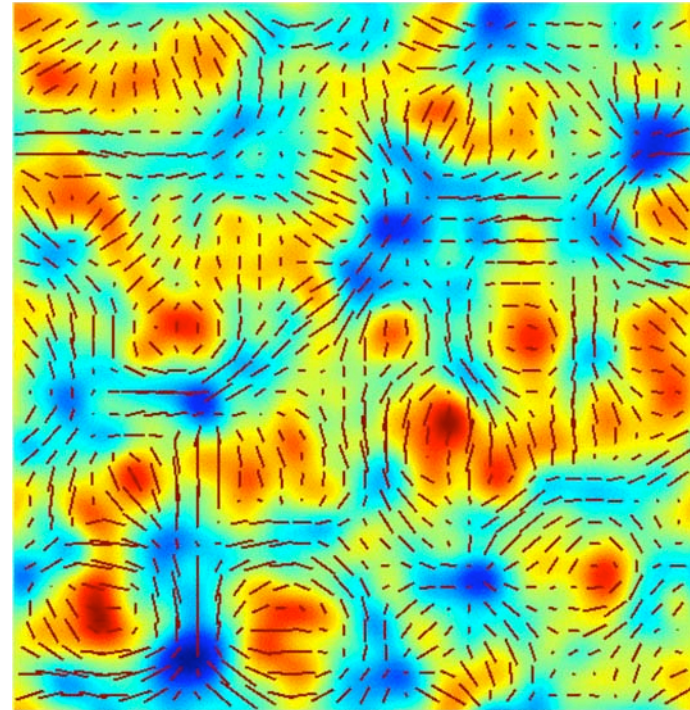
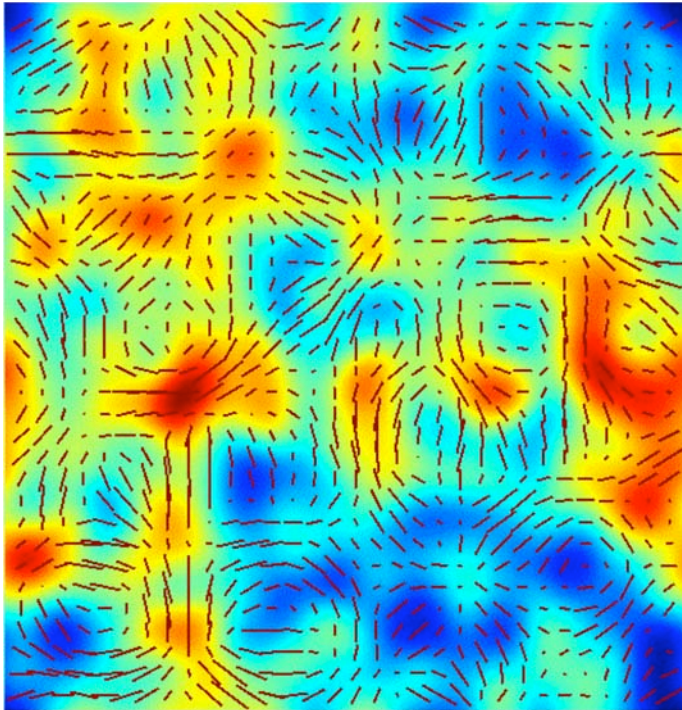
13.7 billion
years



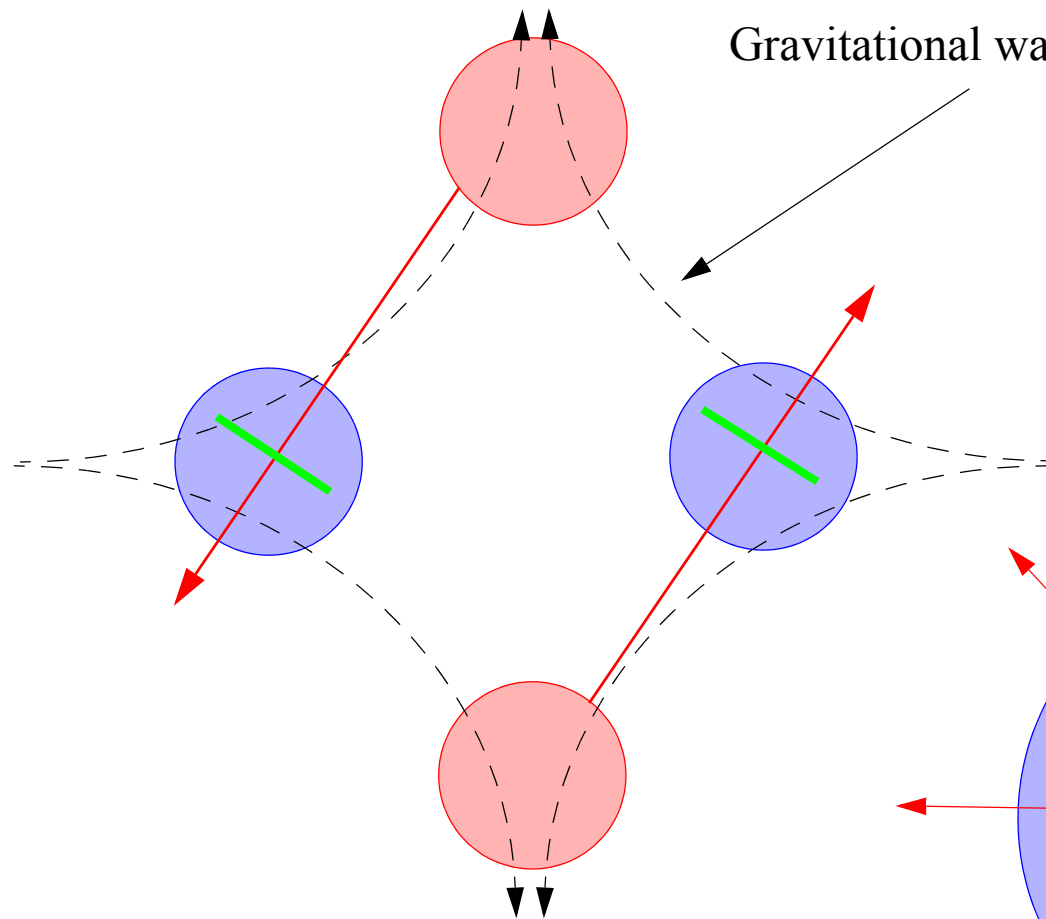




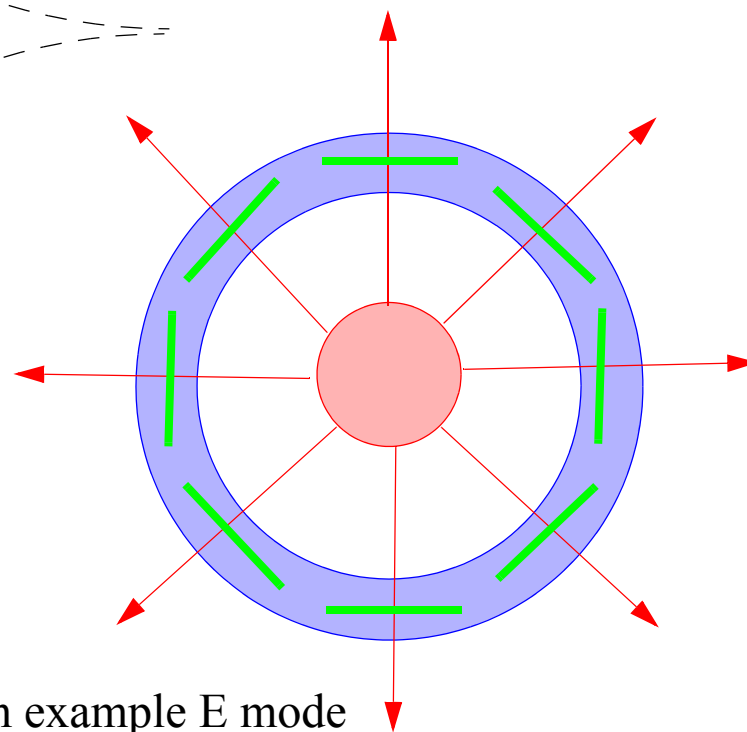
H. Edens



Gravitational wave strain pattern



components of a B mode



an example E mode

